Impact of Micro Silica on the Properties of Porous Calcium Silicate Products

Haastrup, Sonja

DOI (link to publication from Publisher):
10.5278/VBN.PHD.ENG.00035

Publication date:
2018

Document Version
Publisher's PDF, also known as Version of record

IMPACT OF MICRO SILICA ON THE PROPERTIES OF POROUS CALCIUM SILICATE PRODUCTS

BY
SONJA HAASTRUP MERRILD

DISSERTATION SUBMITTED 2018

AALBORG UNIVERSITY
DENMARK

IMPACT OF MICRO SILICA ON THE PROPERTIES OF POROUS CALCIUM SILICATE PRODUCTS

by

Sonja Haastrup Merrild

AALBORG UNIVERSITY
DENMARK

Dissertation submitted 2018

.

Dissertation submitted:	February 2018
PhD supervisors:	Professor Yuanzheng Yue Aalborg University
	Jørgen Mikkelsen Development manager, Skamol A/S
Assistant PhD supervisor:	Associate Professor Donghong Yu Aalborg University
PhD committee:	Associate Professor Morten Lykkegaard Christensen (chair.) Aalborg University
	Professor Tor Grande Norwegian University of Science and Technology
	Senior Specialist and Project Manager Hong Peng Elkem AS
PhD Series:	Faculty of Engineering and Science, Aalborg University
Department:	Department of Chemistry and Bioscience

ISSN (online): 2446-1636
ISBN (online): 978-87-7210-165-1

Published by:
Aalborg University Press
Langagervej 2
DK – 9220 Aalborg Ø
Phone: +45 99407140
aauf@forlag.aau.dk
forlag.aau.dk

Printed in Denmark by Rosendahls, 2018

ENGLISH SUMMARY

Skamol A/S produces calcium silicate for thermal insulation systems. The two key raw materials used in the production of calcium silicate are quicklime (QL) and micro silica (MS). QL is obtained by calcination of limestone, whereas MS is a by-product of the silicon and silicon-alloy production. QL and MS react in water to form a C-S-H gel (from cement notation, C=CaO, S=SiO_2 and H=H_2O), after reaction the C-S-H gel is pressed to boards and autoclaved. The C-S-H gel crystallizes in the autoclave. The quality of raw materials, especially MS from different production sites, highly influences the calcium silicate product properties. The major raw material impact is on bulk density, crystal structure, cold compressive strength and linear shrinkage. To obtain a steady production process, with uniform product properties, it is necessary to better understand how MS influences the product properties of calcium silicate.

In this work MS from different production sites is characterized. It is found that the chemical composition, crystallization temperature and crystal content vary among the as-received MS types. The different MS types are dispersed in water and the particle size, zeta potential and the electrical conductivity of the suspensions are determined.

The difference in reaction rate of different MS types and their influence on the calcium silicate product properties are investigated by varying reaction and autoclave time. The autoclave time highly impacts the crystallinity of the calcium silicate product. Increasing the reaction time leads to decreased bulk density and enhance the crystal formation in the autoclave. The crystal structure influences the cold compressive strength and linear shrinkage of the material. The cold compressive strength is found to be related to the bulk density, but indeed also to the crystal content. A high crystal content results in a high cold compressive strength.

Impact of iron on the calcium silicate product properties is investigated by adding iron ions during reaction and after reaction. When iron is present during reaction, the C-S-H gel formation is hindered. Iron is found to influence the crystallization in the autoclave when added after prereaction. Generally, impurities are found to affect the thermal stability of the calcium silicate.

Particle size and impurities of the MS have strong impact on the reaction rate of the QL-MS reaction. Small particle size and low impurity content is desired for fast reaction rate, which will lead to low density and low thermal conductivity. The reaction time can be varied to obtain same the calcium silicate product properties with MS with different particle size and/or impurity degree. Lastly, impurities should be avoided when high temperature stable products are desired

DANSK RESUME

Skamol A/S producerer calciumsilikat til isoleringssystemer. Råmaterialerne i produktionen af calciumsilikat er brændt kalk (CaO) og mikrosilika (SiO_2). Brændt kalk fås fra brænding af kalksten og mikrosilika er et restprodukt fra produktionen af siliciummetal og siliciumlegeringer. I produktionen af calciumsilikat dispergeres mikrosilika først i vand. Derefter tilsættes brændt kalk, og CaO og SiO_2 reagere i vandet og danner en gel. Denne gel filter presses til plader og pladerne autoklaveres. Under autoklaveringen krystalliserer pladerne. Råmaterialerne påvirker calcium-silikatprodukternes egenskaber, især mikrosilika fra forskellige produktioner påvirker egenskaberne. Produktegenskaber der især påvirkes er rumvægt, tryk styrke og lineære svind ved opvarmning. For at opnå en stabil calciumsilikatproduktion er det vigtigt at forstå, hvordan mikrosilika påvirker calciumsilikatprodukternes egenskaber.

Mikrosilika fra forskellige producenter (forskellige typer) er undersøgt for kemisk sammensætning, krystallinsk indhold og krystallisation ved opvarmning. Under calciumsilikat produktionen dispergeres mikrosilika i vand, derfor er det også vigtigt at kende mikrosilikas egenskaber i vand. Således er partikelstørrelse, zetapotentiale og elektrisk ledningsevne af dispergeret mikrosilika undersøgt.

Reaktionsraten varier når forskellige mikrosilika typer anvendes i produktionen af calciumsilikat. Denne indflydelse på calciumsilikatproduktet er undersøgt ved at variere reaktions og autoklavetiden. Autoklavetiden påvirker krystalstrukturen af calciumsilikatproduktet. Øget reaktionstid resulterer i lavere rumvægt og fremmer krystaldannelsen i autoklaven. Krystalstrukturen påvirker trykstyrke og det lineære svind.

Indflydelsen af jern på reaktionen mellem mikrosilika og brændt kalk er undersøgt ved at tilsætte jernioner under dispergering af mikrosilikaen og efter reactionen mellem SiO_2 og CaO. Resultaterne viser, at jern hindre CaO-SiO_2 reaktionen, hvilket leder til lav krystaldannelse. Når jern tilsættes efter reaktionen påvirker det krystallisationen i autoklaven. Når jern tilsættes før og efter reaktionen resulterer det i sænket styrke og termisk stabilitet. Jern virker også som flux ved høje temperaturer, hvilket resulterer i yderligere sænkning af termisk stabilitet.

I dette arbejde er det konkluderet at partikelstørrelse og urenheder af mikrosilika påvirker calciumsilikatproduktegenskaberne. Små partikler og lavt indhold af urenheder giver hurtigst reaktionsrate, som vil resultere i lav rumvægt og lav varmeledningsevne. Reaktionstiden kan varieres for at opnå samme calciumsilikat-produktegenskaber når mikrosilika med forskellig partikelstørrelse og/eller indhold af urenheder anvendes som råmateriale. Som sidste bemærkning bør urenheder undgås, når calciumsilikatproduktet skal anvendes til høje temperaturer.

ACKNOWLEDGEMENTS

This thesis has been submitted for assessment in partial fulfilment of the PhD degree. The thesis is based on published scientific papers listed in section 1. The PhD is conducted as an industrial PhD under the Innovation Fond Denmark (Grant no. 4135-00090B), in cooperation with Aalborg University and Skamol A/S. The work is conducted at the research laboratory of Skamol A/S and at the Section of Chemistry at Aalborg University. The thesis is not in its present form acceptable for open publication but only in limited and closed circulation as copyright may not be ensured.

I would like to thank my supervisor Yuanzheng Yue, who has made this PhD possible for me. Without his believe in me and guidance the last years, I could not have started and finished this work. Also, a thank to my co-supervisor Donghong Yu for guidance regarding laboratory analysis and discussion of data. Further, my fellow PhD students at Aalborg University, who are always ready to help solving problems in the laboratory or with interpretation and discussion of data. To Rasmus R. Petersen for countless discussions regarding XRD data and general help in the laboratory.

At Skamol I have always felt welcome and a part of the team. In the R&D department a special thank is given to Niels Vilsen and Kim G. Poulsen for help and performance of experiments. Thanks to Bianca Jørgensen, Kim Siefert and Jørgen Mikkelsen for valuable discussions and comments to papers and thesis. Having a group of people with such extensive knowledge and competences to ask and discuss with has been priceless. At last, Alexander Van Lelieveld must be acknowledged and remembered for his great ideas, inputs and inspiration. He had an ability to apply his great knowledge on all kinds of problems. Paper IV is an outcome of his idea. He taught me not to see elephants, when they are not there.

Acknowledgement goes to Elkem Materials for valuable discussions regarding micro silica and for taking me around their laboratories and silicon plants. A special thanks to Bjørn Myhre, for taking his time to answer my many questions regarding micro silica and for supplying different micro silica types tested throughout the thesis.

I would like to thank my family for being who they are and acknowledge my sister Linda Haastrup Sheeran who helped with grammar check of the thesis. Finally, a special thanks to my husband Christian Haastrup Merrild who always believe in me and supports me.

TABLE OF CONTENTS

CHAPTER 1. INTRODUCTION

Skamol A/S produces porous calcium silicate, which is a material used for thermal insulation. The two key raw materials used in the production of porous calcium silicate are quicklime (QL) and micro silica (MS). QL is obtained from calcination of limestone, and MS is a by-product from the silicon and silicon alloy production. The raw materials highly influence the product properties of calcium silicate, and it is the purpose of this project to get a better understanding of the raw material influence.

Calcium silicate is used in technical insulation systems, both in buildings and in high temperature environments. Important product properties for these applications are high compressive and bending strength, high thermal stability, low bulk density and low thermal conductivity. These factors are all influenced by the raw materials used in the production and the processing conditions [1].

Overall the production process of the calcium silicate produced by Skamol A/S takes place in two steps. The first step is the prereaction of MS and QL in water, forming a C-S-H gel (from cement notation: C=CaO, S=SiO_2 and H=H_2O), and the second step is the steam assisted crystallization of C-S-H gel into tobermorite and xonotlite in the autoclave. The steam assisted crystallization takes place at temperatures above 180 °C for xonotlite crystallization [2,3]. In **Figure 1-1** a flow diagram of the production process is shown.

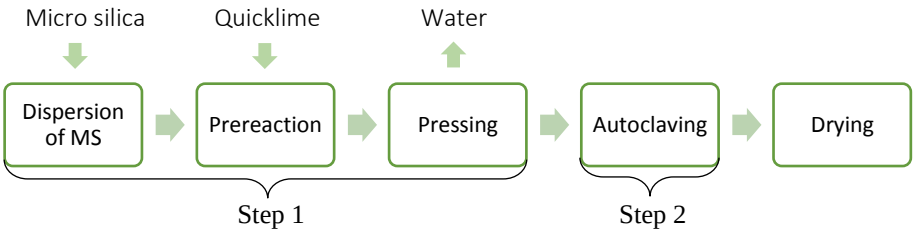

Figure 1-1 *Flow diagram over the calcium silicate production process used at the Skamol A/S plant in Branden, Denmark.*

In the prereaction, QL and MS react forming an amorphous C-S-H gel [1]. The dissolution of silica is very important in the reaction between CaO and SiO_2, since the dissolution rate of SiO_2 is believed to be the rate determining step of the CaO-SiO_2 reaction [4]. Therefore, amorphous silica (e.g. MS) results in faster reaction compared to crystalline silica (e.g. quartz), as it dissolves easier [5,6]. The dissolution of silica proceeds as shown in **Eq. 1-1**.

$$\boldsymbol{SiO_2\,(s) + 2H_2O\,(l) \leftrightarrow H_3SiO_4^-(aq) + H^+(aq)} \qquad \textbf{1-1}$$

The dissolution of silica in water is dependent on pH, temperature, specific surface area and the presence of ions [7]. Since the dissolution of SiO_2 is believed to be the rate determining step of the CaO-SiO_2 reaction, the overall polymerization reaction of SiO_2 and CaO in H_2O can be described as seen in **Eq. 1-2** [4].

$$n_1 SiO_2(s) + n_1 Ca^{2+}(aq) + n_2 OH^-(aq) \leftrightarrow n_1 CaO\ SiO_2\ n_2 H_2O(s) \qquad \textbf{1-2}$$

This product is overall called C-S-H gel [8], which is an amorphous or nanocrystalline material when produced at atmospheric pressure [9].

After prereaction, the C-S-H gel is filter pressed to boards and hydrothermally treated in an autoclave, where the steam assisted crystallization takes place. The C-S-H gel crystallizes into xonotlite and tobermorite, depending on the Ca/Si ratio, the temperature in the autoclave and other factors.

1.1. BACKGROUND AND CHALLENGES

Skamol A/S has produced calcium silicate since 1983, and the production is optimized to increase the quality and output since the factory was founded. High quality, stable production and cost-effectivity are important factors to stay among the best calcium silicate producers in the world.

Skamol A/S strives to have second and preferably third suppliers of raw materials, to ensure stable deliveries and low prices. This results in ongoing search for alternative raw materials. In **Figure 1-2** bulk density (BD) and cold compressive strength (CCS) of 4 calcium silicate samples produced with two different types of MS (MS1 and MS2) and two different types of QL (QL1 and QL2) are seen. The chemical composition of the two types of MS are very similar (~96 wt% SiO_2).

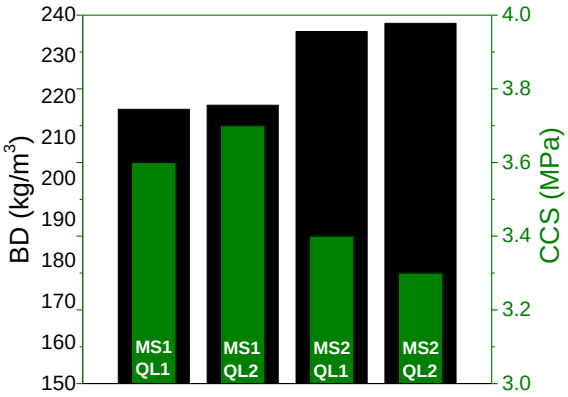

Figure 1-2 *Bulk density (BD) in black and cold compressive strength (CCS) in green of calcium silicate produced with two different types of MS (MS1 and MS2) and two different types of QL (QL1 and QL2).*

From **Figure 1-2** it is found, that calcium silicate produced with same MS, but with different QL displays similar properties. Comparing BD and CCS of the two calcium silicate samples with different MS and same QL a larger difference is found. MS1 results in low BD and high CCS, whereas MS2 results in high BD and low CCS. This shows that the type of MS applied highly influences the properties of the calcium silicate product. Calcium silicate products are sensitive toward changes in raw materials, and especially changes in MS supplier. This results in challenges when alternative raw materials are introduced to the production.

MS is a by-product from the silicon and silicon-alloy production, and varies in chemical composition, particle size distribution, and other factors, among production sites or even among different furnaces at the same plant. This is a challenge when acquiring alternative raw materials for the calcium silicate production. Therefore, information regarding MS characteristics influencing the calcium silicate product properties is important to obtain a steady production of calcium silicate.

1.2. OBJECTIVES

The overall objective of this project is to study the influence of MS on the porous calcium silicate product properties. Further, knowledge regarding which MS characteristics that influence porous calcium silicate product properties is desired.

Different types of MS are characterized to investigate how MS from different suppliers and/or production plants differ. Throughout the thesis and Paper I through IV, these different types of MS are used in the investigation of the MS influence on the calcium silicate product properties:

- The reaction kinetics between QL and MS are investigated to compare the reactivity of two types of micro silica. Different reactivities of MS are expected to lead to different product properties. It is desired to optimize the required reaction time for each MS type, when the reactivity of the individual MS is known.
- The influence of reaction and autoclave time is investigated to determine which processing conditions influence which product properties.
- The impurity content of MS from different production plants varies. Therefore, the influence of impurities is investigated. The focus is on iron, due to the high number of ferro silicon plants in the world.
- Finally, an overall understanding of MS characteristics influencing calcium silicate product properties is desired.

1.3. THESIS CONTENT

The thesis is based on experiments conducted at Aalborg University and at the R&D laboratory of Skamol A/S. Part of the work is published as papers in international peer reviewed journals and one is published as a conference proceeding. Results concerning processing conditions are another part of the thesis, which are not published.

The papers are listed below and cited with roman numbers throughout the thesis.

I. S. Haastrup, D. Yu, Y.Z. Yue. Impact of surface impurity on phase transitions in amorphous micro silica, J. Non-Cryst. Solids 450 (2016) 42-47
II. S. Haastrup, M.S. Bødker, S.R. Hansen, D. Yu, Y.Z. Yue, Impact of amorphous micro silica on the C-S-H phase formation in porous calcium silicates, J. Non. Cryst. Solids. 481 (2018) 556–561
III. S. Haastrup, D. Yu, Y.Z. Yue, Impact of minor iron content on crystal structure and properties of porous calcium silicates during synthesis, Mater. Chem. Phys. 205 (2018) 180–185
IV. S. Haastrup, B. Jørgensen, D. Yu, Y.Z. Yue. Impact of Micro Silica Surface Hydroxyl Groups on Calcium Silicate Products, 60th International Colloquium on Refractories (2017) 222–224

CHAPTER 2. RAW MATERIALS

The two key raw materials used in the production of calcium silicate at the production facility at Skamol A/S are quicklime (QL) and micro silica (MS). The two raw materials are known to impact the calcium silicate product properties, as shown in **Figure 1-2**. In the following sections, the state-of-the-art of both QL and MS is examined along with characterization of commercial types of QL and MS. Since MS is known to have the greatest impact on the calcium silicate product properties, a larger number of MS are tested, and extensive analysis methods are conducted.

2.1. QUICKLIME

Quicklime is an important raw material in the production of calcium silicate. QL is obtained from the decomposition of limestone, which is a natural mineral found in many forms throughout the world. The first use of lime is dated back to 7000 years BC, for production of mortars and plasters [10]. The production of QL has been studied extensively by many researchers. The decomposition process of limestone is complex, and the extensive research in the decomposition process occurring in limestone and the properties of QL is still not fully linked [11,12]. In the following section, the basic knowledge regarding QL will be examined.

Limestone and related rocks are the most frequently used raw material in industry [12]. The chemical composition is typically calcium carbonate and magnesium carbonate (calcite, dolomite, magnesite). The nature of limestone is very complex, consisting of varying sizes of crystals and impurities, changing the textural structure of the minerals [11]. Limestone is formed by the reaction between carbon dioxide and dissolved calcium ions, either by direct precipitation or formed by organisms building shells, skeletons and secrete [13].

Quicklime is produced by the thermal decomposition of limestone ($CaCO_3$) into quicklime (CaO), see **Eq. 2-1**.

$$\boldsymbol{CaCO_3}\ (\boldsymbol{s}) \xrightarrow{\boldsymbol{heat}} \boldsymbol{CaO}\ (\boldsymbol{s}) + \boldsymbol{CO_2}\ (\boldsymbol{g}) \qquad \textbf{2-1}$$

The calcination of limestone is highly endothermic, and the theoretical energy required is 1792 kJ/kg limestone [14] and the temperature required for the calcination of calcite is 900 °C [12]. The thermal decomposition of $CaCO_3$ potentially involves three rate determining steps: heat transfer from the surface through the CaO product, mass transfer of formed CO_2 away from the interface through the product layer, and the chemical reaction seen in **Eq. 2-1** [15]. Which mechanism is the rate limiting has been investigated several times, and there is still not consensus about the results [15–18]. The influence of impurities, crystallinity and microstructure of limestone on the

calcination mechanism is difficult to predict, due to the complex nature of the decomposition of limestone [12].

Industrially the calcining process can take place in vertical shaft kilns or rotary kilns. The kilns can be fired with gas, liquid or solid fuels. A flow of air is induced through the oven to remove the CO_2 produced from the reaction. To prevent too great a pressure-drop over the CaO bed, the limestone pellet size is kept between 5-150 mm, depending on the oven used. The reaction in industrial kilns normally reaches 1000-1300 °C and requires 2-24 hours of reaction, whereas full calcination in the laboratory can be obtained at 900 °C and requires less than 1 min [13,14].

Quicklime is highly porous, and the porosity emerge from the calcination process. During reaction of $CaCO_3$ to CaO the volume decreases, resulting in mechanical stress that leads to fracture of the product. This volume decrease is caused by the CaO crystal growth. The lattice parameters of CaO are different from the calcite crystal structure, leading to tensile stresses within the material. When the CaO crystals reach a critical size, cracks occur [18]. The calcining process and the porosity of the CaO influences the hydration activity. In many applications, the hydration activity is an important property of the CaO product [14]. The hydration reaction of quicklime (see **Eq. 2-2**) is highly exothermic releasing 1140 kJ/kg of CaO [12].

$$\boldsymbol{CaO + H_2O \longrightarrow Ca(OH)_2} \qquad \textbf{2-2}$$

The hydration activity of quicklime varies from seconds to several minutes and can be determined from the increase in temperature with time. Several factors influence the hydration activity: calcination temperature, specific surface area, gasses present during calcination, etc. [10,19]. A high porosity of the CaO is desired, since this leads to a great surface available for reaction. Some researchers [10] found, that the reactivity is reflected in the specific surface area of the quicklime. Shi *et al*. [20] specify that the microstructure of CaO crystals formed during reaction/heating results in the different hydration activities among different types of quicklime.

The microstructure of CaO is highly related to the calcination temperature. The lower the calcination temperature applied, the higher a hydration activity of quicklime is obtained. Calcination at higher temperatures results in sintering of the CaO. If temperatures of 1800 °C and higher are reached, highly sintered CaO is obtained with low surface area. Highly sintered QL is referred to as dead burned lime, due to the low hydration activity [13,19]. Impurities present in the lime can enhance the sintering of the CaO, by acting as fluxing agents decreasing the melting temperature of CaO.

The CO_2 partial pressure highly influences the hydration activity of CaO. Valverde *et al.* [16] found that a high CO_2 partial pressure causes grain agglomeration of CaO. The crystallite size is also increased by the high CO_2 partial pressure, due to adsorbed CO_2 molecules which promote aggregation of metastable nano crystallites, stabilizing

the growth of larger stable CaO crystallites [16]. Presence of H_2O and SO_2 gases during calcination is also found to influence the structure of the quicklime product [19].

QL is a highly complex material and a deeper understanding of the material is beyond the scope of this PhD thesis.

2.1.1. CHARACTERIZATION OF QUICKLIME

The quicklime used in the production of calcium silicate at the plant at Skamol A/S is a light burned QL, to ensure a high CaO activity of the QL. The CaO activity of the QL is an important property, which is a measure of the CaO available for reaction. The presence of calcite and dead burned CaO will both lower the CaO activity of the QL [10]. The CaO activity is determined according to the standard EN 459-2:2010, where QL is dissolved in sugar water and titrated with an acid. The CaO activity of QL used for calcium silicate production is normally in the range from 90-95 %. In the following section two types of commercial QL are characterized with an CaO activity of 94.9 % and 92.2 %.

The crystal structure of the two types of QL is detected by X-ray diffraction (XRD), see **Figure 2-1** (left). From the XRD powder pattern it is seen that the main crystal phase in the two QL types is CaO with traces of calcite ($2\theta = 29.4°$). Traces of calcite will be present when the quicklime is light burned. In hard burned quicklime no calcite will be left and instead larger crystals and sintered CaO will be formed. The intensity of the calcite peak is slightly higher for the QL with 92.2 % active CaO, whereas the intensity of CaO peak of QL with 94.9 % active CaO is highest.

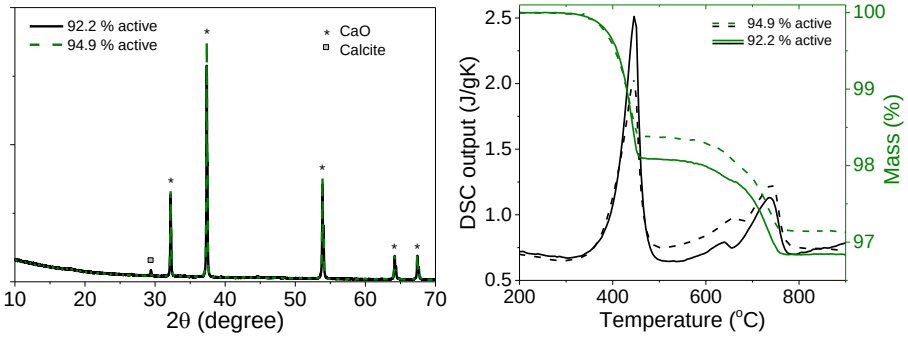

Figure 2-1 *Left: XRD powder pattern of two commercial light burned quicklime types. Right: DSC (black) and TGA (green) scans of two different commercial light burned quicklime types.*

Differential scanning calorimetry (DSC) and thermal gravimetric analysis (TGA) are performed, on two different types of commercial quicklimes, to investigate the phase transition in the CaO (**Figure 2-1**, right). Exothermic peaks are found at 445 °C and again at ~660 °C and 735 °C. The peak at 445 °C is due to water bound as $Ca(OH)_2$

[21], which also corresponds with the weight loss seen from the TGA curve. $Ca(OH)_2$ is crystalline [22], however, no sharp diffraction is found for $Ca(OH)_2$ in the XRD powder pattern. This indicates that the quantities of $Ca(OH)_2$ are low. The hydration of CaO into $Ca(OH)_2$ can take place in some of the production steps or during transportation and storing of quicklime. The following peaks at ~660 °C and 735 °C are the decomposition of calcite, where CO_2 is released corresponding with the weight loss in the TGA curve. The presence of calcite is also observed with XRD.

Slight differences between the two different types of QL are found. The results show that the QL with 92.2 % active CaO contains more $Ca(OH)_2$ than QL with 94.9 % active CaO (**Figure 2-1**, right), seen by the larger area of the endotherm peak at 445 °C on the DSC upscan curve. From the XRD powder pattern, it is found that the calcite content of QL with 92.2 % active CaO is larger than that of the QL with 94.9 % active CaO. This corresponds with the DSC scan, where the area of the endotherm peak at ~735 °C is also slightly larger for the QL with 92.2 % active CaO.

2.2. MICRO SILICA

Micro silica (MS) is an amorphous material, which is used in many different applications, i.e. cement additive, coatings and raw material for insulations [23–27]. MS is a by-product from the production of silicon and silicon alloys in electric arc furnaces [28]. In the production of silicon metal, high purity quartz is reduced to silicon at temperatures up to 2000 °C. The overall reaction is described in **Eq. 2-3** [29]. Several intermediate reactions take place in the furnace, one involves the formation of SiO (**Eq. 2-4**). The SiO is either reduced to SiC (**Eq. 2-5**) or escapes with CO, which at the top of the furnace is oxidized to SiO_2 and CO_2 (**Eq. 2-6**). At the top of the furnace the SiO_2 has no time to rearrange, and so the amorphous nature of the MS is created. Only a few of the reactions that take place in the furnace are listed in **Eq. 2-3** to **2-6**.

$$\boldsymbol{SiO_2(quartz) + C \rightarrow Si(metal) + CO_2\,(g)} \qquad \textbf{2-3}$$

$$\boldsymbol{SiO_2(quartz) + C \rightarrow SiO(g) + CO(g)} \qquad \textbf{2-4}$$

$$\boldsymbol{SiO\,(g) + C \rightarrow SiC\,(s) + CO(g)} \qquad \textbf{2-5}$$

$$\boldsymbol{SiO\,(g) + CO\,(g) + O_2(g) \rightarrow SiO_2\,(s) + CO_2(g)} \qquad \textbf{2-6}$$

After the furnace the oxidized SiO_2 is captured in filter bags, and a fine powder is obtained. The SiO_2 fume consists of spherical amorphous particles, see **Figure 2-2**. After collection from the filter bags, the MS can be densified mechanically or pneumatically to obtain a higher density for easier handling and cheaper transportation [25].

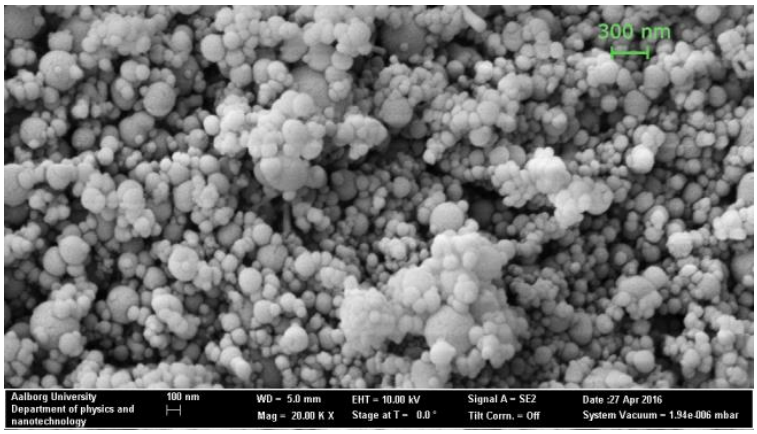

Figure 2-2 *Secondary electron microscopy (SEM) micrograph of as-received MS. MS consists of spherical SiO_2 particles, with traces of impurities.*

Traces of impurities, such as metal oxides and alloys, sulfur and carbon are normally present in the MS. The impurities normally originate from the reducing agents like wood chips and coal. Crystalline impurities, such as silicon carbide, quartz and cristobalite can also be present in the MS [30]. These impurities origin from reactions in the furnace and escape with exhaust gases. The purity content of the MS will depend on the raw materials, processing method and conditions. The MS by-product from the production of ferrosilicon will typically contain a higher degree of impurities compared to MS by-products from the silicon production.

2.3. CHARACTERIZATION OF MICRO SILICA

MS from different production sites is shown to react differently in contact with QL to form calcium silicate, as seen in **Figure 1-2**. Therefore, it is of interest to characterize MS from different production sites and determine which MS properties are desired to obtain high quality calcium silicate for insulation.

There are many silicon and silicon alloy factories around the world, and there are as many different types of MS, with different characteristics. The manufactures often use the chemical composition of MS to categorize the MS. The chemical composition can be determined by X-ray fluorescence (XRF) or titration. Other characteristics are also of great importance, e.g. specific surface area, particle size distribution, surface charge, crystalline impurities, crystallization characteristics and possibly more. Which MS characteristics that influences the calcium silicate product properties are not known.

In this work 11 different MS types from different suppliers and/or factories are characterized. One of the MS types are tested both as densified (D) and as undensified (U), a total of 12 MS types are tested. The chemical composition is measured by XRF either by the supplier or in the laboratory of Skamol A/S see **Table 2-1**. In the laboratory of Skamol A/S the XRF measurements (Epsilon 3x, PANalytical, Netherlands) are performed on fused beads. Approximately 0.6 g of dry MS is mixed with 6.0 g of lithium borates ($Li_2B_4O_7$ and LiBO, Claisse), and the mixture is melted at 1100°C.

Table 2-1 *Chemical composition of 12 different types of MS, from different suppliers and/or plants. U is undensified and D is densified. The chemical composition is determined by XRF and is given in wt %.*

ID	SiO_2	Na_2O	K_2O	MgO	CaO	Al_2O_3	Fe_2O_3
983U*	96.9	0.05	0.68	0.24	0.37	0.13	0.01
971U*	97.8	0.09	0.21	0.16	0.21	0.14	0.04
971D*	97.4	0.09	0.18	0.15	0.24	0.18	0.06
970D	97.1	0.02	0.57	0.06	0.30	0.12	0.06
968U*	96.7	0.11	0.58	0.4	0.26	0.47	0.17
955U*	96.5	0.15	0.62	0.44	0.26	0.26	0.1
958D*	95.8	0.03	0.70	0.14	0.48	0.20	0.24
952D	97.5	0.2	0.49	0.2	0.2	0.2	0.1
950D*	96.5	0.15	0.48	0.2	0.32	0.25	0.06
935D	93.1	0.06	0.67	0.21	0.75	1.50	1.27
928D	92.8	0.41	1.40	0.98	0.36	0.81	2.24
903D	90.3	0.66	1.75	1.35	0.17	0.66	0.63

*XRF data from supplier

Impurities are expected to be present as metals/alloys, metal oxides and/or salts. Low concentrations of impurities are present in MS, therefore, it is difficult to determine which state the impurities are in.

Impurities are an important factor when characterizing MS, but other MS properties are also of interest to understand the reactivity of MS. In the following sections, crystallites present in as-received MS, the crystallization behavior upon heating, particle size distribution, zeta potential and electrical conductivity are determined of the different types of MS listed in **Table 2-1**.

2.3.1. CRYSTALS IN MICRO SILICA

Despite the amorphous nature of MS, traces of crystals can be present, e.g. cristobalite, quartz and silicon carbide (SiC) [23,30,31]. In **Figure 2-3** the XRD powder patterns of the 10 different types of MS are shown. At 2θ~17-26° a broad peak is found, which is characteristic for amorphous silica [32]. This broad peak has been explained by

periodic short-range order of silica [33]. At 2θ = 21.9° the (101) peak for cristobalite [34] is found and at 2θ=26.6° the (101) peak for quartz [35] is found. Both cristobalite and quartz are found in sample 958D, 952D, 950D and 928D. At 2θ=35.6° and 59.9° the (111) and (220) peaks, respectively, for SiC are found. Traces of SiC is found due to the intermediate reaction in the furnace, as described in **Eq. 2-5**. SiC is present in all samples, showing different intensities (amount of SiC). Beside quartz, cristobalite, and SiC, sample 903D also show traces of other crystals, which most likely is metal oxides or alloys of some kind [Paper I].

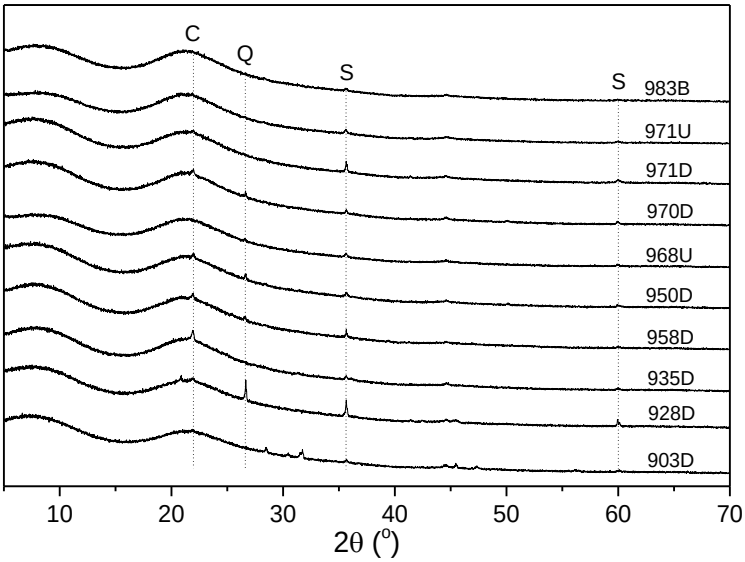

Figure 2-3 *XRD powder pattern of different types of micro silica origin from different production sites and methods (C is cristobalite, Q is quartz and S is silicon carbide). The intensities in Y-axis are shifted vertically for clarity.*

The XRD powder patterns in **Figure 2-3** show, that only some MS types contain traces of quartz and cristobalite. When MS escapes through the top of the furnace, it is possible that quartz and cristobalite crystallites also escape. Therefore, it is likely that cristobalite and quartz are present in all samples, but in such low quantities that it is not possible to detect with the XRD method. The difference in crystal concentration among the MS is likely to be caused by the different production methods.

2.3.2. CRYSTALLIZATION IN MICRO SILICA

Silica is a very stable glass former [36], however, upon heating of MS, it is possible for surface nucleation to take place [37,38]. Several crystal structures of silica exists, of which tridymite, cristobalite and quartz are formed at atmospheric pressure [39]. The crystallization of silica is strongly induced by the presence of impurities, especially alkali metal oxides, e.g. Na_2O [39,40]. Upon heating, impurities work as

nucleating agents and break up the silica network structure, lowering the energy barrier of crystallization [41].

The crystallization behavior of MS is investigated using differential scanning calorimetry (DSC), see **Figure 2-4**. DSC is performed on 11 of the 12 MS samples, in argon atmosphere (STA Jupiter 449C, Netzsch). A baseline (blank) and sapphire are measured. 25 mg of MS sample is weighed off in an alumina crucible. The samples are heated to 1300 °C with a scan rate at 20 K/min and subsequently downscanned with a cooling rate at 20 K/min to 400 °C. A second up/down scan is performed on the same sample.

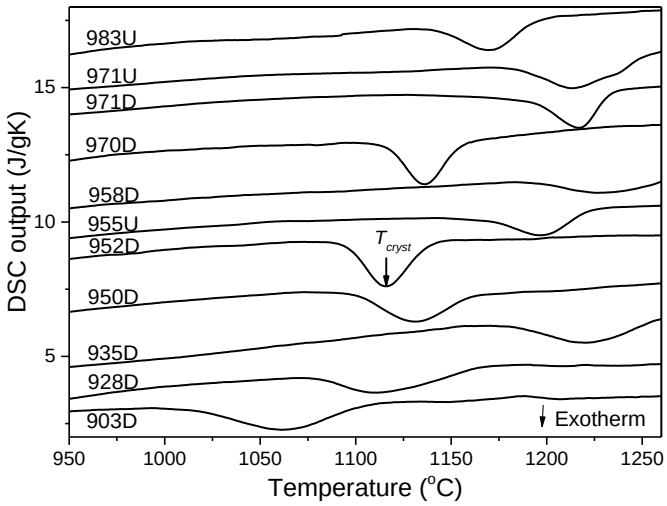

Figure 2-4 *DSC up-scan of 11 MS samples. The exothermic peak (T_{cryst}) is crystallization of amorphous micro silica to cristobalite. The Y-axis is shifted vertically for clarity.*

From **Figure 2-4** it is found that all 11 samples have a clear exotherm peak, with the peak temperature varying from 1061 to 1226 °C. These temperatures are referred to as the characteristic temperature of crystallization, T_{cryst} and are listed in **Table 2-2** for all MS tested by DSC. The amorphous MS crystallizes into cristobalite. This is confirmed by the second up-scan, where all samples exhibit an endotherm in the interval of 220-250 °C, which is characteristic for the α to β phase transition of cristobalite. This second up-scan does not vary much among different MS samples [Paper I].

The position of T_{cryst} is dependent of the impurity content, both chemical and crystalline impurities. An amorphous material containing structural heterogenous domains or foreign ions will have a higher tendency to crystallize than a homogenous matrix. The foreign ions work as nucleating agents and fluxing agents, hence lowering the energy barrier for nucleates to grow [Paper I]. In **Figure 2-5** T_{cryst} as a function of

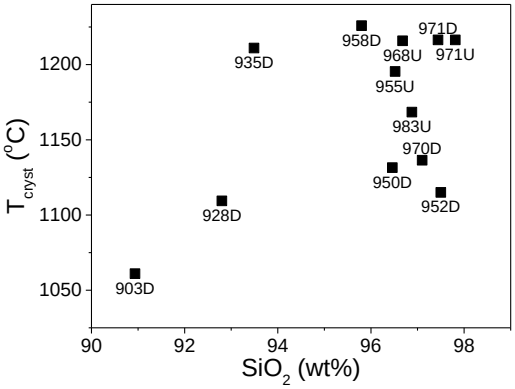

Figure 2-5 *Crystallization temperature (T_{cryst}) as a function of SiO_2 content for 13 different types of MS.*

SiO_2 content for each MS is plotted, where it is found that at low SiO_2 content T_{cryst} is low. At higher SiO_2 content no trend is found, which shows that not only the chemical impurities influence T_{cryst}, but also the crystalline impurities. 958D is the MS with highest T_{cryst}, however, the SiO_2 content is lower than several other MS types and from XRD it is found that crystallites are present. So T_{cryst} cannot be predicted simply by determining the chemical and crystalline impurities.

It is expected that the crystallization takes place on the surface of the MS particles and that the impurities are mainly present between MS particles (**Figure 2-6** a) or on the MS surface (**Figure 2-6** b). This is expected due to the strong glass forming ability of silica [38,42]. Silicon and oxygen organizes into a tetrahedral structure, where the oxygens are referred to as bonding oxygen. The number of bonding oxygens are expressed by the Q^n notation. Q^n represents the silica tetrahedron and *n* denotes the number of bridging oxygen sites per tetrahedron [43]. In the bulk of an MS particle, a tetrahedron will be linked to 4 oxygens and designated as Q^4. On the surface of the silica particle surface hydroxyl groups or siloxane groups will be present [44], therefore, the energy barrier of crystallization is lowest on the silica surface. Foreign ions depolymerize the silica tetrahedron network creating non-bonding oxygens, which will also lower the energy barrier of crystallization [45].

T_{cryst} of 958D and 935D are higher than the other MS types, compared to the relatively high impurity content of the two. If impurities are present as particles between MS particles instead of directly on the surface, as illustrated in **Figure 2-6** (a), then the impurity particles will have less contact with MS particles with the same impurity content, compared to if the impurities are distributed on the surface of the MS particles (**Figure 2-6** (b)) or reacted with the silica surface. The larger the impurity particles between MS particles are, the higher will the T_{cryst} be relative to the amount of impurities. The peak shape of 958D and 935D are broader than the other MS with higher SiO_2 content. A broad peak results when different energy barriers throughout

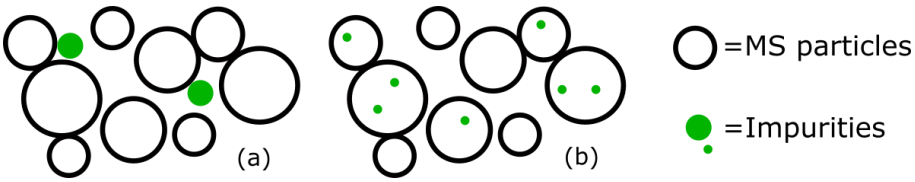

Figure 2-6 *MS particles with (a) impurity particles between MS particles and (b) impurities present on the surface of MS particles.*

the MS are present [Paper I]. Difference in energy barrier throughout the MS is related to the size distribution of impurities among MS particles and the location of the impurities. If the impurities are evenly distributed on the MS surface and all particles contain equal impurities compared to the surface area, then the energy barrier of crystallization will be the same throughout the sample. This will lead to a sharp crystallization peak. If the impurities form clusters on the MS particles (**Figure 2-6** b), or are present as impurity particles between MS particles (**Figure 2-6** a), a broader temperature range of crystallization will result. The less distributed the impurities are, the broader will the resulting crystallization peak be. Comparing this with the results in **Figure 2-4**, it is inferred that the impurities of 935D and 958D are non-uniform and mainly located as impurity particles between MS particles. The same degree of non-uniformity is also found for 903D and 928D, whereas 950D and 955D are slightly more uniform, but still less uniform than the remaining MS types.

These results show, that the presence of impurities highly varies among MS from different production sites. The DSC results can give an indication of how the impurities are present in the as-received MS.

2.3.3. PROPERTIES OF DISPERSED MICRO SILICA

When different types of MS are dispersed in water, they behave very differently. In **Figure 2-7** 12 different types of MS are dispersed in water using ultra sonication, and the samples are left to sediment for one month. In the bottom of all samples a layer of sedimented MS particles are observed. 955U and 903D are separated into two clear layers with MS particles at the bottom and clear water at the top. The remaining MS samples have an unclear layer between the sediment and the clear water, which most likely are particles in the nanometer range. The water is clear, grey or yellow among the dispersed MS types. The grey color origin form carbon from the MS production process, and the yellow color is expected to origin from organic compounds.

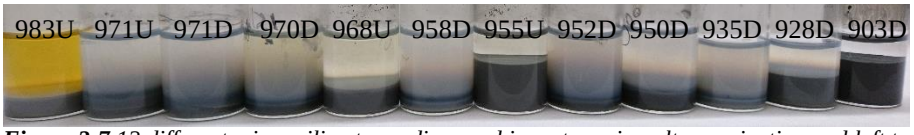

Figure 2-7 *12 different micro silica types dispersed in water using ultra sonication and left to sediment for one month.*

The particle size, zeta potential and electrical conductivity are determined for each suspension, to investigate the sedimentation behavior and colloidal properties of the suspensions in **Figure 2-7**.

Average particle size and zeta potential are determined using a ZetaSizer Nano ZS (Malvern). Particle size is determined by the dynamic light scattering method. 2 g MS is dispersed in 10 mL demineralized water under sonication for 5 min (Ultrasonic processor 500W, model CV334) prior to measurement. From this suspension 1 mL is diluted in 30 mL and transferred to a folded capillary cell (DTS1070, Malvern). Three scans on the same sample are performed for both zeta potential and particle size, and an average of the three scans is calculated, see **Table 2-2**.

In **Figure 2-8** the particle size distribution by volume of 5 MS types is shown as examples. Two peaks are present for all MS types, one in the range from 100-1000 nm (peak 1) and one peak in the range from 3000-5000 nm (peak 2). The average particle size of peak 2 is larger than 3 µm and is therefore assumed to be undispersed MS particles. Since the measurement is stationary, there is a risk that particles in the 3000-5000 nm range sediment during measurement. There is a possibility that undispersed particles break up during reaction, due to the high pH during reaction. The particle size reported in **Table 2-2** is the mean size of peak 1, since the largest surface area available for reaction origin from this fraction.

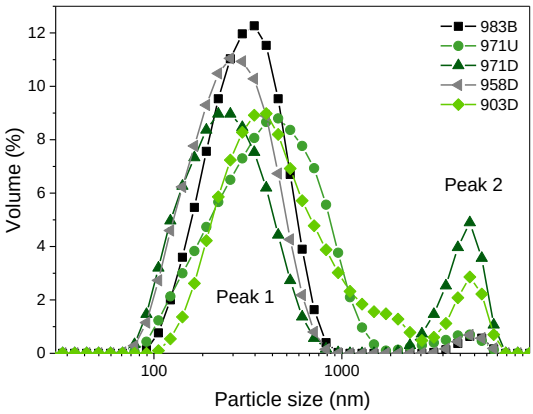

Figure 2-8 *Volume distribution as a function of particle size of 5 different types of micro silica dispersed in water.*

The chemical composition of the different MS types varies, and whether the impurities are alloys or oxides are not known. When dispersed in water MS slowly dissolves, and some impurities also dissolve. All dissolved ions from the MS will contribute to the electrical conductivity of the water-MS system. Therefore, differences in solubility of impurities present on the surface of different MS types can be investigated with electrical conductivity measurements. Electrical conductivity (Seven Multi, Mettler Toledo) is measured on 2.00 g MS suspended in 10.0 mL

demineralized water (electrical conductivity > 1 µS/cm for water) in ultrasonic bath for 1 hour. The measurements are conducted at 23 ± 0.5 °C. It is assumed that the electrical conductivity contribution from silica is similar for all MS types and hence negligible.

Table 2-2 *Silica content, zeta potential (ZP), electrical conductivity (EC), average particle size (size) and characteristic temperature of crystallization (T_{peak}) of the different MS types investigated.*

ID	SiO_2	ZP	EC	Size	T_{peak}
	wt%	mV	µS/cm	nm	°C
983B	96.9	-37	1070	291	1168
971U	97.8	-31	825	347	1216
971D	97.4	-35	722	254	1216
970D	97.1	-39	1251	214	1136
968U	96.7	-39	952	278	1216
958D	95.8	-36	1756	256	1226
955U	96.5	-39	1367	296	1156
952D	97.5	-40	1461	241	1115
950D	96.5	-38	1271	229	1132
935D	93.1	-34	1995	253	1220
928D	92.8	-39	1764	231	1109
903D	90.9	-44	4750	343	1061

From **Table 2-2** it is found that the average size of peak 1 is between 214-347 nm, where the smallest particle size is found for 970D and the largest is found for 971U. In the reaction between MS and quicklime, the dissolution rate of MS is believed to be the limiting step [4]. Therefore, the particle size of MS is a very important property regarding the reactivity of MS. If the particle size is the only factor influencing the reaction rate, then 970D should result in the fastest reaction rate and 971U should result in the slowest reaction rate. However, it is shown that impurities also influence the reaction rate between MS and QL [Paper II]. The surface hydroxyl groups of MS are also expected to influence the reaction rate between MS and QL [Paper IV, 46].

From the SEM micrograph in **Figure 2-2** it is seen, that the single particle size of MS is in the range from ~200 nm down to 5-10 nm, which is smaller than the average particle size reported in **Table 2-2**. The particle size varies with different production sites, due to sintering of the MS particles when MS particles are in direct contact in the hot exhaust gas during production. The sintering in the exhaust gas depends on the concentration of MS particles in the gas and the temperature of the exhaust gas [23]. Such clusters of sintered spheres can be seen by TEM images, see **Figure 2-9** and [23,25,26].

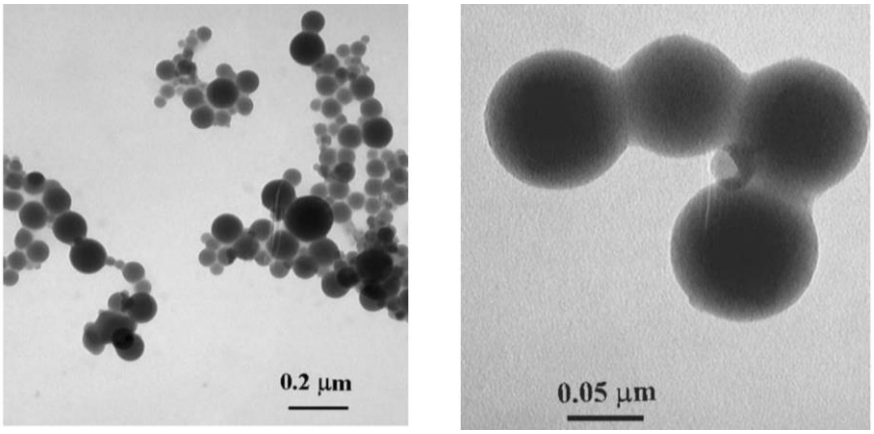

Figure 2-9 *TEM image of sintered clusters of MS. Figure adapted from ref. [25].*

The particle size is also influenced on whether the MS is densified or not. Densified MS is found to be more difficult to disperse in water than undensified MS [23,25]. When the dried MS is stored, the presence of water will highly influence the particle size of MS. Water can react with the surface of MS, resulting in creation of new bonds between surfaces of MS particles in direct contact. This results in almost irreversible aggregation of the MS, and less surface area is available for reaction [39]. This partly irreversible aggregation of MS particles is known as "ageing".

The surface charge of the MS particles could also influence the reaction between QL and MS [Paper IV]. The particle charge is determined as the zeta potential, which is related to the electrical potential around a particle. The zeta potential gives an indication of the stability of the colloidal system, a zeta potential > 25 and < -25 mV should result in a stable system [47]. If particles have low surface charge these particles aggregate, resulting in sedimentation during measurement. Generally, all MS types are below -25 mV and should result in a relatively stable system. 903D is the MS with the most negative zeta potential and shows the highest layer of sediment in **Figure 2-7**. The high sediment layer indicates that the particles have a high charge and cannot aggregate and/or flocculate. Flocculation of particles results in increased particle size, which increase the sedimentation rate. 955U also displays a high sediment layer and a zeta potential higher than average for the MS measured. 971U/D and 935D have the highest zeta potential and display the lowest sediment layer. However, an unclear layer of MS particles is observed above the sediment layer. This can be very small particles and particles with a more negative zeta potential than the average measured for the individual MS types.

The electrical conductivity is expected to be related to the SiO_2 content, since low SiO_2 content is equivalent with a high impurity content. In **Figure 2-10** (left) the electrical conductivity of different MS types is plotted as a function of SiO_2 content.

There is a tendency for electrical conductivity to increase at low SiO_2 content. This is expected since the higher the degree of impurities, the more ions are available for dissolution. The decreasing electrical conductivity as a function of SiO_2 content is not equally clear for all MS types. This could be due to the presence of different types of impurities and difference in solubility of the impurities.

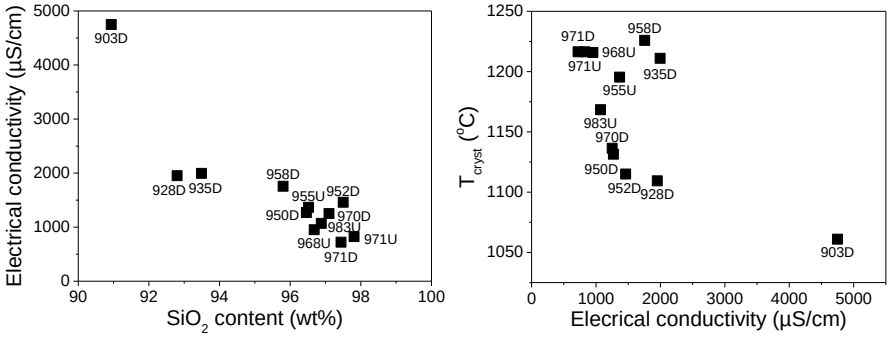

Figure 2-10 *Left: Electrical conductivity of different MS types as a function of their SiO_2 content. Right: T_{cryst} of different MS types as a function of electrical conductivity.*

In **Figure 2-10** (right) T_{cryst} as a function of electrical conductivity is plotted. There is a tendency for T_{cryst} to decrease as the electrical conductivity increases. However, 958D and 935D do not follow this trend. If the impurities of 958D and 935D are present as impurity particles between MS particles as discussed in Section 2.3.2 and illustrated in **Figure 2-6**, then there is a possibility that these impurities are more available for dissolution than the impurities on the surface of MS particles. The correlation of electrical conductivity and T_{cryst} seems to be slightly higher than their individual correlation with SiO_2. This indicates, that the impurities that contribute to lower T_{cryst} are also available for dissolution and contribute to electrical conductivity.

2.4. SUMMARY

In the production of calcium silicate, quicklime and micro silica are used as raw materials. Quicklime is obtained from calcination of lime stone, whereas micro silica is a by-product from the silicon and silicon-alloy productions. Quicklime with different CaO activity is found to differ in crystal content. In this project the focus has been on characterizing micro silica.

The crystal structure of as received micro silica is investigated, and it is found that all types contain traces of SiC, and some also contain traces of quartz and cristobalite. The crystallization behavior is investigated with DSC, and it is found that the micro silica crystallizes into cristobalite upon heating. The crystallization temperature depends on impurity content, crystallites and whether the impurities are present on the micro silica particle surface or as impurity particles between micro silica particles.

The behavior of micro silica in water is also investigated, by determining the average particle size, zeta potential and electrical conductivity. The particle size of micro silica varies depending on production site. Zeta potential is found to influence the stability of the colloidal system. Electrical conductivity is dependent of the impurity content and related to the crystallization temperature.

Characteristics of micro silica are investigated, however, the repeatability of different productions over time of micro silica from the same silicon plant is not investigated. The change in micro silica particle size or crystallization temperature at different production times will give an indication of the stability of the micro silica production. A stable micro silica quality over time is important for the calcium silicate production.

CHAPTER 3. PREREACTION AND CRYSTALLIZATION OF POROUS CALCIUM SILICATES

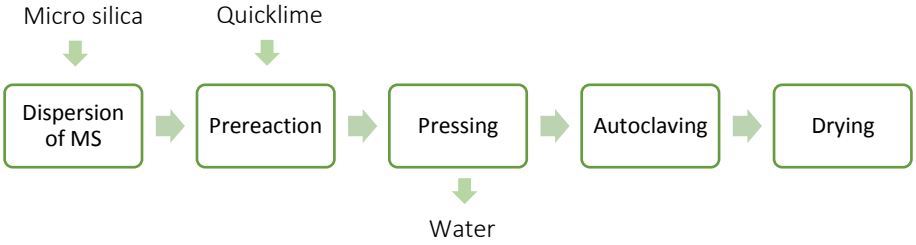

Figure 3-1 *Flow diagram over the calcium silicate production process used at the Skamol A/S plant in Branden, Denmark.*

The overall production of calcium silicate is described in **Figure 3-1**. In the following the reaction between CaO and SiO_2 is described and the influence of prereaction and autoclave time are investigated.

3.1. STRUCTURE OF C-S-H GELS

The prereaction of CaO and SiO_2 before autoclaving is important for the final product properties of the calcium silicate material [48]. Greenberg [4] found that the dissolution of silica is the limiting step in the reaction between silica and CaO. However, the understanding of the reaction between MS and QL is very limited, and the focus has been regarding C-S-H formation during hydration of cement [8,49].

When QL and MS react, the silica organizes into a chain with Q^1, Q^2 and Q^3 sites (Q^n represents the silica tetrahedron and *n* denotes the number of bridging oxygen sites per tetrahedron). The Q^2/Q^1 ratio is a measure of the silica chain length, which is shown to increase with increasing reaction temperature and/or time [1]. The Ca organizes in between the silica chains creating layers consisting of Ca and silica tetrahedron. The prereaction temperature and time influence the crystallization, pore structure and silica chain structure of the C-S-H gel [1]. These factors can also influence the properties of the final calcium silicate product, i.e. thermal stability, strength and bulk specific gravity [1,48].

The C-S-H gel formed in the prereaction is a poorly crystalline material that can vary in Ca/Si ratio. The C-S-H structure is similar to the phases formed during hydration of cement, these phases have intensively been investigated by several scientists [8,46,49–51]. C-S-H gel structure with Ca/Si < 1.5 is found to be similar to the

tobermorite crystal structure, whereas C-S-H gel with Ca/Si > 1.5 is similar to the jennite structure [8,52,53]. The tobermorite structure consists of silica tetrahedra chains in a *dreierketten* formation, with CaO polyhedral layers with Ca^{2+} and H_2O in the interlayers [54]. Different types of tobermorite crystals exist, characterized by their interlayer water resulting in varying length of the c axis (0.9, 1.1 and 1.4 nm). The different types of tobermorite are formed depending on the temperature during synthesis.

After the prereaction the C-S-H gel is filter pressed and autoclaved. In the autoclave the formation of tobermorite ($Ca_5Si_6O_{16}(OH)_2 \cdot 4H_2O$), xonotlite ($Ca_6Si_6O_{17}(OH)_2$), and other types of crystals take place. The kind of crystal formed depends on the Ca/Si molar ratio and autoclave temperature, see phase diagram in **Figure 3-2** [3]. More than 30 stable C-S-H phases have been reported [3].

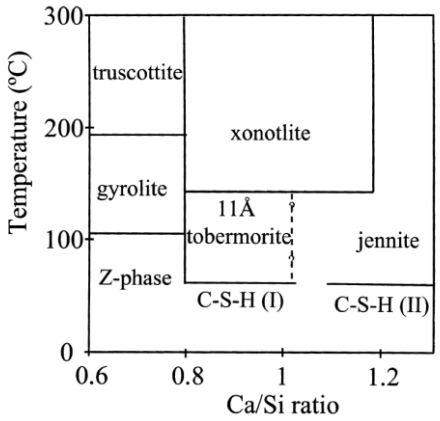

Figure 3-2 *Phase diagram of calcium silicate phases with different Ca/Si ratio and different reaction temperature. Adapted from ref. [3].*

The crystal structure of tobermorite is flake-like and forms in the autoclave when the molar ratio of Ca/Si = 0.8-1.0 [52,55,56] and is even found to be stable at molar ratios > 1 [57]. The reason for the stability in a range of Ca/Si ratios is possibly due to the partly disorder of the tobermorite crystal, which increases with higher Ca/Si ratio [3,58]. Xonotlite is needle-like and this crystal structure forms when the molar ratio of Ca/Si=1 [59,60]. In **Figure 3-3** SEM images of tobermorite sheets and xonotlite needles are seen. The crystallization of C-S-H phases into xonotlite is found to proceed either as an intermediate step where tobermorite is firstly formed and then recrystallizes into xonotlite or as a direct crystallization of C-S-H phases into xonotlite [61–63].

Upon heating the tobermorite and xonotlite crystals are transformed into the needle shaped wollastonite ($CaSiO_3$) crystal at temperatures of 700-800 °C [55,64], see

Figure 3-3 *SEM image of calcium silicate with xonotlite needles, tobermorite sheets and wollastonite needles.*

Figure 3-3. These phase transitions are associated with shrinkage, due to dehydration and change in micro structure. Xonotlite is a hydrated form of wollastonite and both are needle shaped, therefore, less shrinkage is associated with this phase transition, compared to the phase transition from tobermorite to wollastonite [60].

For a product with high thermal stability xonotlite is desired, due to less shrinkage upon heating compared to the tobermorite crystal [27]. Tobermorite is found to have a lower thermal conductivity, therefore this crystal is desired when high insulation values are required. The lower thermal conductivity of tobermorite is likely to be caused by the higher degree of disorder.

3.2. PRODUCTION OF POROUS CALCIUM SILICATES

The production of porous calcium silicates investigated in this work follows the flow diagram shown in **Figure 3-1**. The porous calcium silicate, is produced either on a pilot plant or in laboratory scale. In the following section the two production methods are explained.

On the pilot plant 4 or 8 kg of MS is firstly dispersed in water. A dispersion disc is used in the dispersion of MS. After dispersion the MS suspension is transferred to a reaction chamber with hot water. In the reaction chamber QL is added to obtain a Ca/Si ratio of 1. The suspension is mixed with a propeller stirrer. At this point the C-S-H gel is formed and this process step is called the prereaction. Organic fibers and crushed calcium silicate is dispersed in water in a different tank. This mixture is added to the reaction chamber with C-S-H gel. The slurry with organic fibers and crushed calcium silicate is colder than the reaction mixture, and therefore the C-S-H gel formation is assumed to stop after addition of this slurry. Then the reaction mixture is filter pressed with a fixed pressure. The pressed samples are then autoclaved. After autoclaving the samples are dried.

When producing calcium silicate in laboratory scale 100 g of MS is used. The MS is dispersed using ultrasonication. After ultrasonication the MS is transferred to a beaker with hot water and QL is added to obtain a Ca/Si ratio of 1. The suspension in the beaker is stirred using a magnetic stirring bar. A mixture of organic fibers and crushed calcium silicate is added to the mixture after reaction, resulting in decreased temperature. The reaction mixture is pressed in a different type of hydraulic press. With this press, the height of the samples is controlled instead of controlling the pressure. This is due to limitations in the pressure control of this hydraulic press. After filter pressing, the samples are autoclaved in the same autoclave as samples produced on the pilot plant.

The products obtained from the two methods are not directly comparable. This is due to different method of dispersing the MS, different stirring speed and stirring method during reaction [65] and difference in the filter pressing method.

3.3. PREREACTION AND FORMATION OF POROUS CALCIUM SILICATES

Prereaction and autoclave times are the two main processing steps in the production of calcium silicates, see **Figure 3-1**. Therefore, it is of interest to investigate how varying reaction and autoclave times influence the product properties. The reaction rate of the MS-QL reaction into C-S-H gel will influence the conversion degree, hence, the prereaction time required will be dependent of the reaction rate. It is known that different types of MS result in different reaction rates [Paper II]. How the reaction rate influences the final product properties will be investigated by varying the prereaction time. The impact of varying autoclave time on the calcium silicate product properties are also investigated. Two types of MS are tested, to investigate if the impact of reaction and autoclave time is the same on both types.

3.3.1. VARYING PREREACTION AND AUTOCLAVE TIMES

The prereaction and autoclave time are investigated using two types of MS, 935D and 903D. The particle size and SiO_2 content is 253 nm and 93.5 wt% for 935D and 343 nm and 90.3 wt% for 903D. Additional information regarding the chemical composition of the two MS types is found in **Table 2-1** and the particle size, zeta potential and electrical conductivity are found in **Table 2-2**. The QL used is from the same supplier throughout all experiments, however, from two different batches. The CaO activity is 92.0 % for reactions with 935D and CaO activity is 90.8 % for reactions with 903D.

The samples are prepared on the pilot scale, 4 kg of MS is used for each batch, and the procedure is as described in Section 3.2. The prereaction is split into two parts, first reaction period is mainly for mixing and is fixed to 20 min for all reactions. The second reaction period is with reduced stirring speed for C-S-H gel formation, and

this reaction time varies among samples for 15, 30, 45 and 60 min. The autoclave times are set to 150, 300, and 600 min. The number of batches prepared with each MS is 12. Samples prepared with 935D are referred to as sample CS935 after prereaction and samples prepared with 903D are referred to as sample CS903 after prereaction. The samples are tested for crystalline structure using x-ray diffraction (XRD) and bulk density (BD), cold compressive strength (CCS), modulus of rupture (MOR), and linear shrinkage (LS) at 950 and 1050 °C are determined.

The XRD powder patterns of series CS935 are shown in **Figure 3-4** where those of CS903 are alike and not shown here. The main crystal phase is xonotlite, all samples also contain tobermorite and calcite. The sharpest XRD peaks are found for samples autoclaved for 600 min. Samples autoclaved for 150 min generally display smaller and broader peaks than samples autoclaved for longer times.

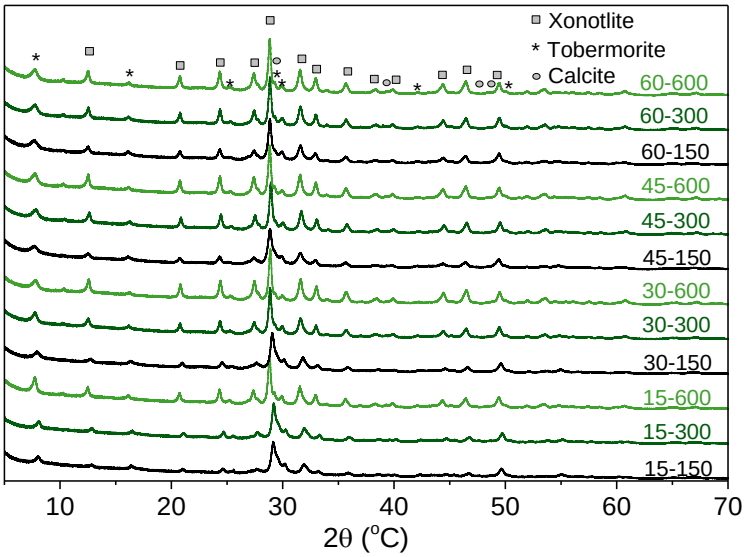

Figure 3-4 *XRD powder patterns of calcium silicate prepared with MS935 at different reaction and autoclave times. The numbers of each powder pattern denote different processing conditions, the first number refers to the prereaction time and the second number refers to the autoclave time in minutes.*

The peak width of the XRD powder pattern is a measure of the crystallite size, the larger the crystallites the sharper and better defined the XRD peaks are. The broad peaks observed for samples autoclaved at 150 min, indicate that the crystallites are small after short autoclave time. With longer autoclave time the XRD peaks become thinner and more defined, hence bigger crystallites are present in the material with longer autoclave time. The peak positions of samples with short reaction time shift towards lower 2θ as the autoclave time increases. Shaw et al. [3] also found a shift in peak position of C-S-H gel, as autoclave time is prolonged or autoclave temperature

is increased. This shift in peak position is explained by the ordering of the CaO octahedral layers which are influenced by the ordering of the silica layers. This ordering is likely to result in increased chain length of the silica *dreierketten*. Increased silica chain length should result in larger crystallites, which correlates with the observed decrease in width of the XRD peaks, corresponding to larger crystallites.

The crystal phases are quantified using the Rietveld refinement method, using quartz as external standard and the analysis program HighScorePlus (Panalytical). The crystallographic information files (CIF) used in the Rietveld refinement are obtained from Churakov and Mandaliev [60] for xonotlite with the space group *P-1*, from Hamid *et al.* [66] for tobermorite with the space group *Imm2* and from Post *et al*. [67] for calcite with the space group *R-3cH* . In *Figure 3-5* the xonotlite and tobermorite fractions are plotted as a function of reaction time at different autoclave times for series CS935 and CS903. For both series the xonotlite content increases with prolonged autoclave time. Samples autoclaved at 150 min have the lowest xonotlite content and is found to slightly increase with increased reaction time. The samples autoclaved at 300 min increase the most with increased reaction time for both CS935 and CS903. Samples from series CS935 autoclaved for 600 min also increase, but already after 30 min of reaction, the maximum xonotlite content is obtained.

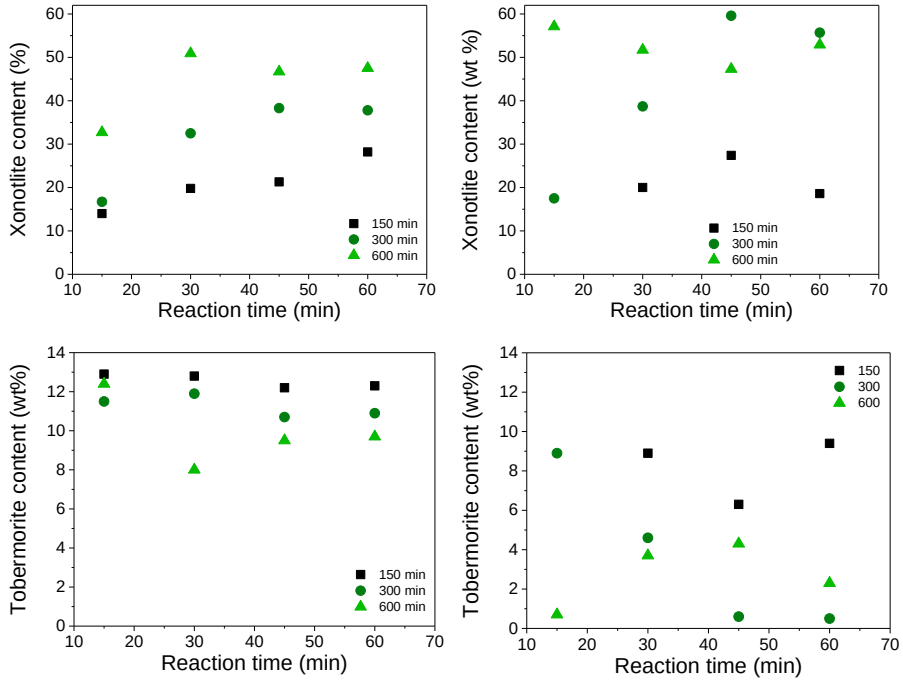

Figure 3-5 *Xonotlite (top) and tobermorite (bottom) of CS935 (left) and CS903 (right) autoclaved at different times as a function of reaction time, samples are autoclaved for 150, 300 and 600 min.*

Generally, it is found that the tobermorite content is higher at autoclave times of 150 min and decreases as the autoclave time is prolonged. The crystallization of C-S-H into xonotlite is suggested to proceed by first crystallizing into tobermorite and then further crystallization into xonotlite [63]. Comparing this with the XRD results, then more tobermorite is present at short autoclave times, and with increasing the time, the tobermorite is transformed into xonotlite. The tobermorite content of CS935 is higher than that of CS903. A Ca/Si molar ratio below 1 will promote tobermorite growth [60,68], therefore, the Ca/Si ratio of series CS935 is expected to be below 1.

With 600 min of autoclaving all samples within same series nearly obtain the same xonotlite content with different reaction times, which indicate that there is a limit of how much xonotlite can be formed with the production method used. For series CS935 the maximum amount of xonotlite obtained is ~50 wt%, whereas for CS903 ~60 wt% of xonotlite is obtained. This difference in xonotlite content could be due to higher tobermorite content in CS935, i.e. less tobermorite is transformed into xonotlite due to the molar ratio.

With reaction time longer than 45 min, there is a tendency for the xonotlite content to decrease, this tendency is especially seen for CS903. This indicates, that longer reaction time does not necessarily result in increased formation of xonotlite. The crystallization pathway in the autoclave can proceed in different ways, two main path ways were discussed by Hsiang and co-workers [1]; firstly the dissolution and re-precipitation and secondly the transformation between solids. Most likely the dominating path way will be dissolution and re-precipitation with short C-S-H chains, and with increased reaction time the chain length increases, and the dominating crystallization pathway changes to be transformation between solids. The dissolution and reprecipitation is expected to take place from the end of the C-S-H chains and from partially or unreacted MS and QL from the prereaction. This crystallization path is expected to be slower, compared to the transformation between solids, since potentially three steps are involved. Firstly, the dissolution involving bond breaking, secondly, the diffusion of ions to the nucleation site, and thirdly, the crystal growth involving bond formation. The transformation between solids proceeds by partial bond breaking changing the bonding angles to a more ordered crystal structure. This path way is expected to be faster, until too long chains are obtained. Too long C-S-H chains will result in entanglement, and thereby ordering of the chains into crystals will be sterically hindered.

At short reaction times, the C-S-H chains are short [1] and more raw material is unreacted during prereaction [Paper II]. At this period, it is expected that the dissolution and reprecipitation is dominating in the autoclave. With increased prereaction time, the C-S-H chain length increases, and the crystallization path shifts to be dominated by transformation between solids. Too long a prereaction time will result in sterically hindered crystallization. Therefore, it is expected that an optimum reaction time exist, in which most xonotlite crystal is formed in the autoclave. This

correlates with the slight decrease in xonotlite content for CS903 at 60 min of reaction, see **Figure 3-5**.

The number of nucleation sites may vary depending on the raw materials used, this is expected to influence the crystal content. A high number of nucleation sites will result in a high number of crystallites, that will grow with longer reaction time. Some of the crystallites formed during autoclaving may be in the nanometer range. A high number of short C-S-H chains will result in a high number of small crystallites. There is a possibility that these small crystallites are X-ray amorphous. Whether some of the amorphous phases determined from XRD are crystallites can be investigated by differential scanning calorimetry (DSC).

In **Figure 3-6** two DSC scans of sample CS935 reacted at 60 min and autoclaved for 150 and 600 min are shown. The DSC scans show a clear endotherm at ~735 °C and ~750 °C for the samples autoclaved for 150 and 600 min, respectively. This is the phase transition of tobermorite and xonotlite to wollastonite. During this phase transition water is lost, seen as the endotherm peak. The sample autoclaved for 150 min further has an exotherm peak at ~850 °C, which is the phase transition of amorphous C-S-H phases into wollastonite. The energy of amorphous phases is higher than that of crystal phases, and therefore energy is released when crystallization takes place. No exotherm peak is present for CS935 reacted for 60 min and autoclaved for 600 min, even the XRD results indicate that there are ~40 wt% amorphous phase in this sample. This shows that some of the crystallites in the calcium silicate material are nanocrystalline, and therefore not detected by XRD.

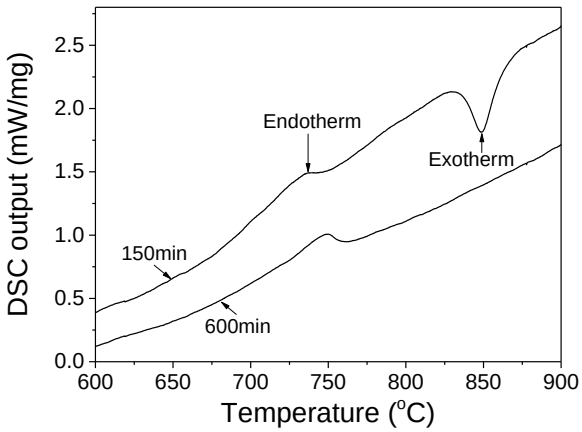

Figure 3-6 *DSC scan of two samples from series CS935 reacted for 60 min and autoclaved for 150 and 600 min.*

The BD is plotted as a function of prereaction time in **Figure 3-7**. BD is measured at least two times for each batch. It is clearly seen, that BD decreases with increased prereaction time for both series. Increased reaction time results in increased C-S-H

gel formation [Paper II]. The development of C-S-H gel is expected to create the porosity of the material, since it is found that the surface of the gel increases with time [1]. This correlates with the results found in **Figure 3-7**, where increased reaction time results in lower BD, i.e. higher porosity. In Paper II it is also found, that the degree of C-S-H gel formation varies among different types of MS. This is also found in **Figure 3-7** where the BD of CS935 generally is lower than BD of CS903, at the same reaction and autoclave time. This indicates that 935D react faster with QL than 903D does. The particle size of 903D is larger than 935D, and the degree of impurity is higher, two factors which are found to influence the reaction between MS and QL [PaperII, 4]. Therefore, it is likely that CS903 react slower than CS935.

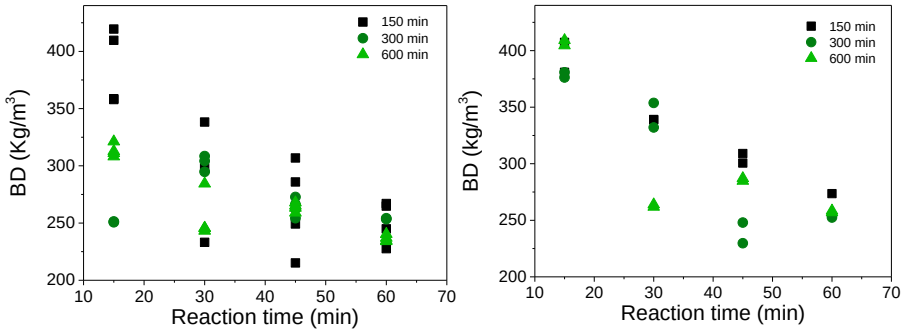

Figure 3-7 *Bulk density (BD) of CS935 (left) and CS903 (right) as a function of reaction time, samples are autoclaved for 150, 300 and 600 min.*

From **Figure 3-7** it is also found, that samples autoclaved at 150 min, generally has a higher BD than samples autoclaved for longer periods, at the same reaction time. This is especially seen in series CS935. The boards are shaped prior to autoclaving, therefore, only shrinkage of the material during drying can have an influence on the BD. This indicates that too short autoclave time results in shrinkage during drying after the autoclaving process.

Tobermorite can exist as a normal and anomalous type, where loss of water at about 300 °C results in shrinkage of normal tobermorite whereas the anomalous type does not [56,69]. El-Hemaly *et al.* [69] found that the anomalous tobermorite is present when longer autoclave time is applied. The anomalous tobermorite is further found to be an intermediate in the crystallization of xonotlite. The autoclave time of 150 min may result in formation of the normal tobermorite, and when dried after autoclaving shrinkage occurs. This will result in stresses internally in the material, and if the stress difference exceeds the strength of the gel network cracks will occur [70]. Samples autoclaved at 150 min and short reaction times have higher crack formation after drying, than samples autoclaved and reacted for longer times. After longer autoclave

time the anomalous tobermorite may form and less shrinkage upon drying takes place, and more xonotlite is formed with time.

Cold compressive strength (CCS) of series CS935 and CS903 autoclaved at different times are plotted as a function of reaction time in Figure 3-8. Series CS903 is found to decrease in CCS with increased reaction time for samples autoclaved at 150 and 300 min and slightly increase in CCS for samples autoclaved at 600 min. Series CS935 autoclaved for 150 min is also found to decrease with increased reaction time, whereas samples autoclaved at 300 and 600 min slightly increase. It is known that a high BD is correlated with a high CCS, however, the crystal structure and size also influence CCS. The samples of CS935 and CS903 with a high strength are also found to have a high density. These samples are also found to have a higher amorphous phase (~50 wt % or more), which indicates that when the amorphous phase dominates high CCS is obtained at high BD. It is observed that samples with high amorphous content also has a higher tendency of crack formation. Series CS935 autoclaved at 300 and 600 min generally has a higher CCS compared to series CS903, even BD is slightly lower. This could be due to higher crystalline content and a higher number of small crystals contributing to the strength.

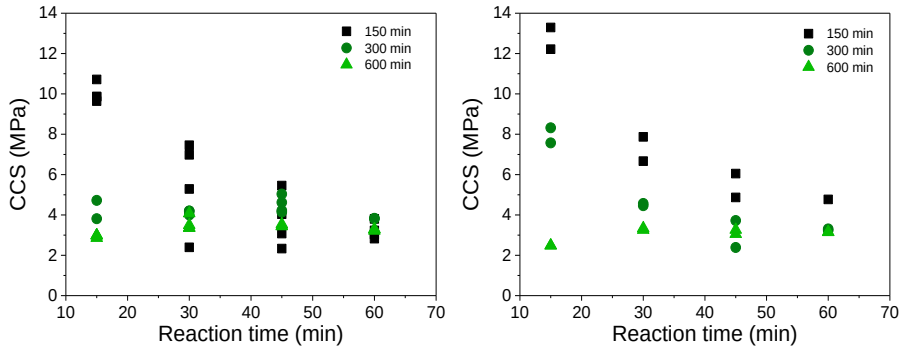

Figure 3-8 *Cold compressive strength (CCS) of CS935 (left) and CS903 (right) as a function of reaction time, samples are autoclaved for 150, 300, and 600 min.*

In **Figure 3-9** modulus of rupture (MOR) of series CS935 and CS903 autoclaved at different times are plotted as a function of reaction time. For both series samples reacted for 15 min generally have a lower MOR, however, a high degree of scattering is observed indicating a high uncertainty on the measurement. This indicates that processing conditions and type of MS only slightly influence MOR. Organic fibers are added, which are expected to contribute to a higher MOR.

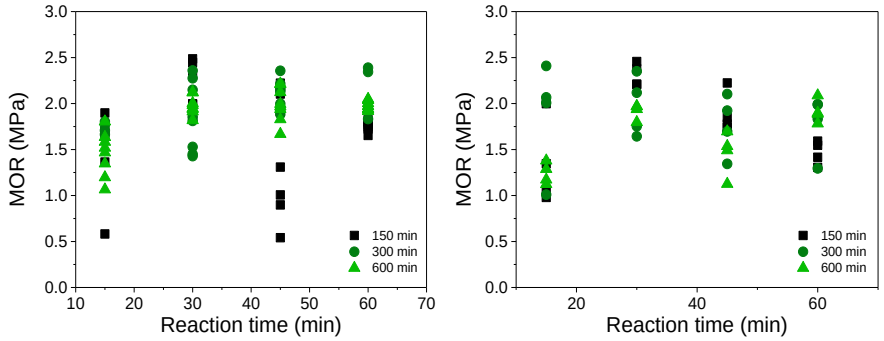

Figure 3-9 *Modulus of rupture (MOR) of CS935 (left) and CS903 (right) as a function of reaction time. The samples are autoclaved at 150, 300 and 600 min.*

The linear shrinkage is determined at 950 and 1050 °C and plotted as a function of reaction time in **Figure 3-10** for CS935 and CS903. When the samples crack after heating, it is not possible to measure the length, and therefore no shrinkage is determined for cracked samples. Samples reacted and autoclaved at short times have a higher tendency to crack. LS of CS935 is generally higher than LS of CS935 at 950 °C and at 1050 °C the shrinkage is generally higher for series CS903. The higher LS of CS935 at 950 °C could be due to the higher tobermorite content of this series.

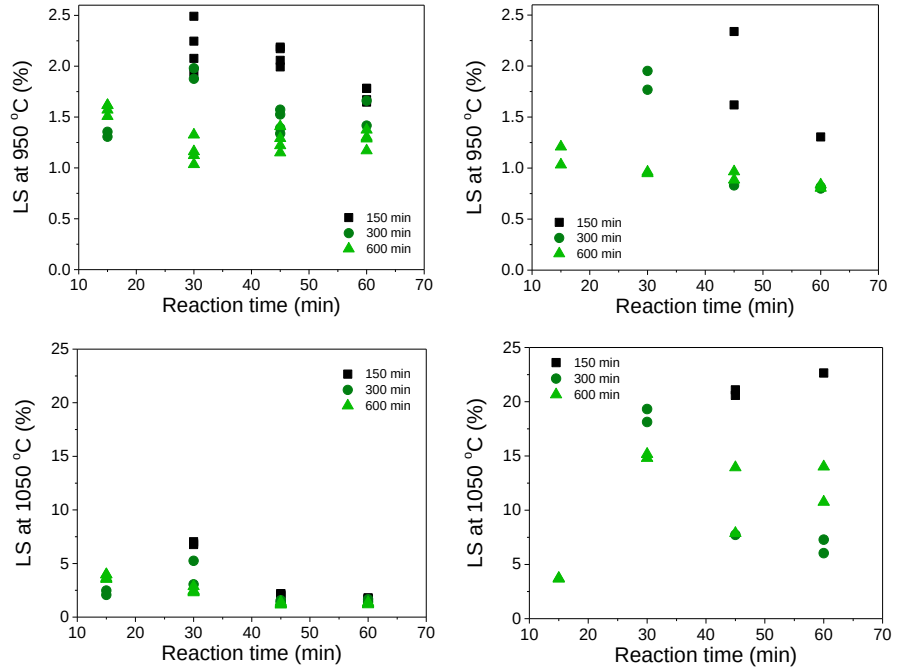

Figure 3-10 *Linear shrinkage (LS) of CS935 (left) and CS903 (right) determined at 950°C (top) and at 1050°C (bottom) as a function of reaction time, samples are autoclaved at different times.*

For both series, there is a tendency for LS to decrease with increased autoclave time when heated to 950 °C and there is also a slight tendency for LS to decrease with increased reaction time. The presence of xonotlite improves the thermal stability, and from **Figure 3-5** it is found that increased autoclave and reaction time result in increased xonotlite crystal formation. Therefore, the lower LS with longer autoclave and reaction time is most likely due to more xonotlite present in the samples. This tendency is not as clear for LS determined at 1050 °C. At 1050 °C the calcium silicate material starts to sinter and other mechanisms than the phase transition induced shrinkage influence the LS. The sintering process is influenced by the presence of impurities working as fluxing agents [Paper III]. The chemical composition of the two types of MS are very different. The impurity content is higher for 903D, which is also the series with the highest shrinkage at 1050 °C. This indicates that impurities highly influence LS of calcium silicate at temperatures above 1000 °C.

3.4. SUMMARY

To investigate how reaction and autoclave time influences the final product properties, experiments with varying reaction and autoclave times are conducted. These experiments show that both reaction and autoclave time highly influences the calcium silicate product properties. With increased autoclave and/or reaction time the xonotlite content increases. With increased reaction time bulk density decreases. Cold compressive strength is mainly influenced by the crystal composition and bulk density, and so it is only indirectly dependent of reaction and autoclave time. For both series modulus of rupture is not influenced by reaction and autoclave time. Linear shrinkage decreases with increased xonotlite content, but increases when more impurities are present in the MS.

These results clearly show that different raw materials react differently. Therefore, it is highly important to understand the reaction kinetic of new types of MS for calcium silicate production. In the production of calcium silicate, the reaction time is normally fixed to a certain time for reaction. This will result in different product properties when different MS types are used in the production. If the reaction kinetic is determined for new MS types, the required reaction time of MS and QL, to obtain the same product properties in every production, can be obtained.

CHAPTER 4. STRENGTH OF POROUS CALCIUM SILICATES

With application of calcium silicate in heavy industries, high cold compressive strength (CCS) is often required, due to heavy loads during use. A high modulus of rupture (MOR) is also important for easy handling of the material, so the material does not break before or during installation. As found in Chapter 1, MOR is mainly dependent of the type of fibers used. CCS is very dependent on the bulk density (BD) but also on a well reacted and crystallized calcium silicate material.

Calcium silicate produced with different types of MS results in different product properties. BD and CCS are normally correlated, i.e. a high BD results in a high CCS. However, some MS types result in calcium silicate with low BD and high CCS, as illustrated in **Figure 1-2**. It is important to get a better understanding of strength development in calcium silicate products, to determine which factors that influence the strength of calcium silicate materials.

4.1. RAW MATERIAL IMPACT ON STRENGTH

The prereaction of C-S-H gel is performed on the pilot plant as described in Section 3.2. and the filter pressing is performed on the small press, which is normally used for laboratory scale samples. 5 samples of equal volume are taken from the reaction slurry and filter pressed to different thicknesses, leading to different BD. After filter pressing, the samples are autoclaved and dried. Calcium silicate samples are produced with MS958, MS952 and MS903 as raw material, and the CaO activity of the QL is 90.8 % for all reactions. After reaction the samples are referred to as CS958, CS952 and CS903 in the following section. BD and CCS are determined with double determination, and the crystal content is determined with XRD using Rietveld refinement and external standard, as explained in Section 3.3.

In **Figure 4-1** CCS as a function of BD is plotted for CS958, CS952 and CS903. It is seen that CCS of CS958 and CS952 is increasing linearly with BD in the range tested. The slope of the two samples are different, indicating that the strength evolution with BD of the calcium silicate products are different when produced with the two MS types. At low density CCS of CS952 is slightly higher than CS958, however, the tendency changes as BD increases. This shows that the highest CCS at low BD is obtained with MS952, however, if a high BD with high CCS is desired, then MS958 is preferred. CCS of CS903 as a function of BD does not follow a linear trend and CCS is generally lower than CS958 and CS952 at same BD.

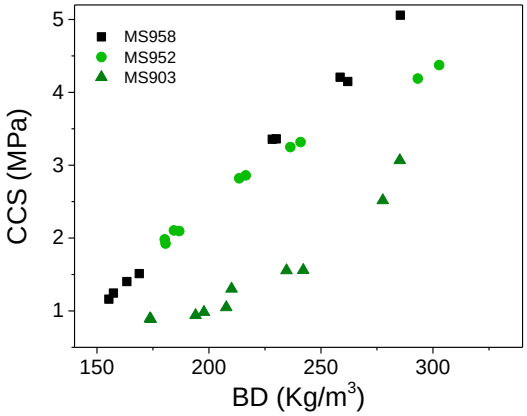

Figure 4-1 *Cold compressive strength (CCS) as a function of bulk density (BD), for CS958, CS952 and CS903.*

The XRD powder patterns of CS958 and CS903 are shown in **Figure 4-2**. The XRD powder patterns of series CS952 and CS958 are similar, therefore, only CS958 is shown as an example. The figures show that the main phase formed is xonotlite with traces of tobermorite and calcite. The intensity of the peaks varies between CS958 and CS903, indicating that less xonotlite is present in CS903. The peaks of CS903 are slightly broader, indicating that the crystallites formed in this material is smaller than those in CS958.

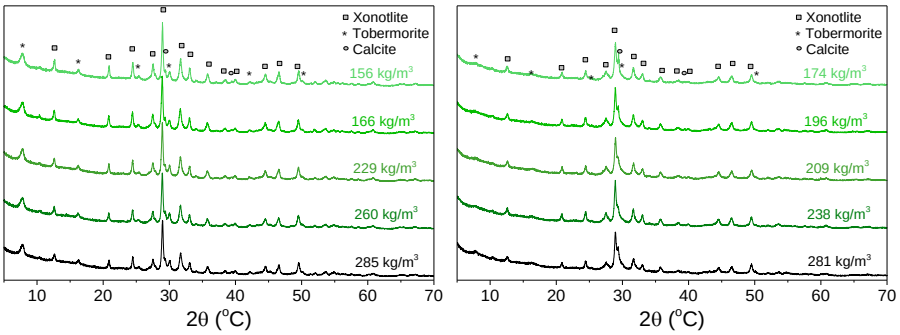

Figure 4-2 *XRD powder pattern of series CS958 (left) and CS903 (right) pressed to different densities.*

The phases are quantified using the Rietveld refinement method, see **Figure 4-3**. The xonotlite content varies among the three calcium silicate samples, the highest content is found for CS952 and the lowest is found for CS903. The highest CCS at low BD and lowest amorphous content is found for CS952 followed by CS958 and finally CS903. This indicates that a high crystal content results in high CCS at low BD.

CS958 has a lower xonotlite content than CS952, however, the amount of total amorphous phase is similar for the two samples, see **Figure 4-3** (right). CCS of the two samples are within the same range, indicating that crystal phases (both xonotlite and tobermorite) contribute to CCS. In Paper IV the strength is also found to increase when the tobermorite content increases, resulting in increase of total crystal phase. The amorphous phase is found not to contribute to CCS, for CS952 and CS958. CCS of CS903 increases with BD, even the crystal structure is stable. This indicates that when BD is high, a high CCS can be obtained with dominating amorphous phase.

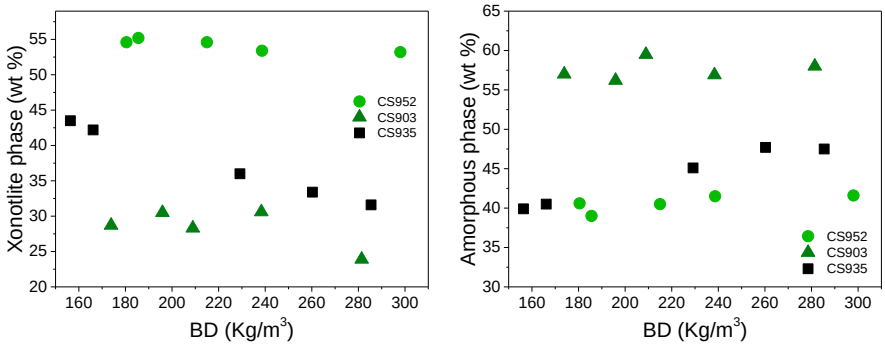

Figure 4-3 *Xonotlite (left) and amorphous phase (right) of CS958, CS952 and CS903 as a function of bulk density (BD). The phases are quantified from XRD powder patterns using the Rietveld refinement method and external standard.*

The xonotlite content of CS958 decreases with increasing BD. For CS952 and CS903 the xonotlite content is stable throughout the tested BD. The reason for this decrease in xonotlite phase with increasing BD for CS958 is not known.

4.2. SUMMARY

In this chapter, C-S-H gel is reacted on the pilot plant and filter pressed in laboratory scale. The bulk density is varied by changing the pressing height. We find that cold compressive strength increases with increasing bulk density. Cold compressive strength is also found to be dependent of the crystal structure of the calcium silicate. The crystal structure is determined with XRD and quantified using the Rietveld refinement method. It is found that high crystalline content generally results in high strength.

The increase in cold compressive strength with increasing bulk density is not the same for different types of MS. The reason for this difference in correlation between cold compressive strength and bulk density among micro silica types is not determined. The size of the crystallites in the calcium silicate material, can be the reason for this difference. It is of interest to investigate the crystallite size to determine the correlation of crystallite size with CCS.

CHAPTER 5. IRON IMPACT ON POROUS CALCIUM SILICATES

Former investigations indicate that impurities influence the calcium silicate product properties [PaperIII, 2, 61, 68, 71]. Iron present during reaction between MS and QL is found to highly influence the crystal structure, cold compressive strength and linear shrinkage of the synthesized calcium silicate [Paper III]. In the following sections, the impact of iron present during prereaction of calcium silicate produced with two different types of MS is investigated. Further it is investigated how iron influences the crystallization in the autoclave.

5.1. IRON IMPACT ON PREREACTION OF POROUS CALCIUM SILICATES

The type of MS used in the calcium silicate production highly influences the properties of the material, as shown in **Figure 1-2**. Therefore, the impact of iron on calcium silicate produced with a second MS is compared with the results from Paper III. In Paper III 952D is used for calcium silicate production (CS952). To compare the iron impact on calcium silicate produced with another MS sample, calcium silicate with 971D is prepared with different iron concentrations (CS971). 971D is chosen due to the high SiO_2 content and low iron concentration. The production follows the procedure described in the experimental section of Paper III.

The Ca/Si and Fe/Si molar ratios of the calcium silicate samples are found using XRF, see **Table 5-1**. The Ca/Si ratio of CS952 is 0.98-0.96, whereas for CS971 the ratio is deviating from 1.09 to 0.91. This large span in Ca/Si ratio of CS971 will most likely influence the crystal structure. When Ca/Si < 1 tobermorite will be present along with xonotlite, and since the Ca/Si ratio decreases with increasing Fe/Si the tobermorite content will increase. From the XRF measurements it is also found, that the Fe/Si ratio of the reference sample is lowest for CS971, implying that less iron is present in this type of MS. Generally, all samples contain less iron than added, indicating that some iron is lost during filter pressing of the calcium silicate samples.

Less iron is incorporated in the CS971 samples, with the same amount of iron added. It is expected that iron is present interstitially in the C-S-H gel network [PaperIII]. Therefore, increased C-S-H gel polymerization should result in a higher amount of iron captured in the C-S-H gel matrix. A higher polymerization degree of the C-S-H gel with the same reaction time is obtained with a fast reaction rate of the MS [PaperII]. This indicates that the reaction rate of 952D is faster than that for 971D, due to the higher incorporation of iron in the matrix of CS952. In **Table 2-2** the particle size of the two MS types is shown. The average particle size of 971D and

952D are found to be 253 nm and 241 nm, respectively. Further 971D is observed to be more difficult to disperse than 952D, seen by the large volume fraction of peak 2. The smaller particle size of 952D is expected to result in a faster reaction [4], which corresponds with the observations that more iron is incorporated in the C-S-H gel network of CS952.

Table 5-1 *Molar ratios of Ca/Si and Fe/Si of CS952 and CS971 determined from XRF. Results for CS952 is taken from Paper III.*

ID	CS952		CS971	
	Ca/Si	Fe/Si	Ca/Si	Fe/Si
Ref	0.98	0.00052	1.09	0.00032
Fe0.1	0.98	0.00077	0.96	0.00053
Fe0.5	0.98	0.00175	0.94	0.00139
Fe0.7	0.97	0.00199		
Fe1.0	0.97	0.00301	0.92	0.00247
Fe1.3	0.96	0.00377		
Fe2.0			0.91	0.00461

The XRD powder patterns of CS971 and CS952 with iron added are seen in **Figure 5-1**. The crystal structure of both references is mainly xonotlite, CS952 further contains tobermorite. No tobermorite is present in the reference of CS971, which agrees with the Ca/Si > 1 found from the XRF results. The xonotlite content decreases as Fe/Si increases, and more amorphous phase is present. The decrease in xonotlite phase with increasing Fe/Si is very comparable for CS971 and CS952, which show that the influence of iron on the crystal structure is the same, even two different types of MS are applied.

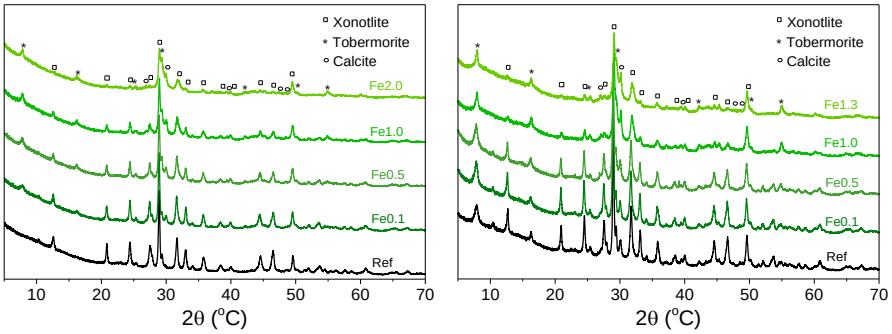

Figure 5-1 *XRD powder pattern of calcium silicate with varying concentrations of iron. Left: CS971. Right: CS952, modified from Paper III.*

Differential scanning calorimetry (DSC) is performed by heating the sample to 1000 °C with a scan rate of 20 K/min. In **Figure 5-2** (left) the DSC scans of 5 samples from

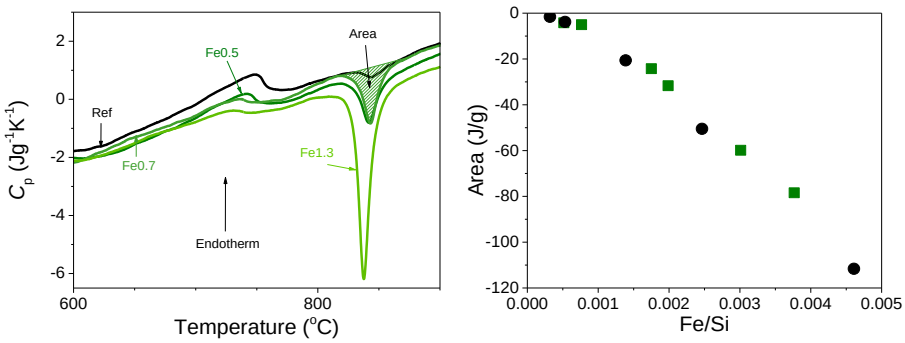

Figure 5-2 *Left: DSC scan of CS952 with different iron concentrations. Right: area of the exotherm peak of both CS952 (square) and CS971 (circle). Results for CS952 are adapted from Paper III.*

series CS952 are shown as examples. The endotherm in the DSC scan is the phase transition from xonotlite to wollastonite, where water evaporates from the xonotlite structure [Paper III]. The temperature of this phase transition is seen to slightly decrease, with higher concentrations of iron. The exotherm signal is crystallization of amorphous phase into wollastonite crystal. In **Figure 5-2** (right) the area of the exotherm peak found from the DSC scan is plotted as a function of Fe/Si for CS952 and CS971. The exotherm peak area increases with increasing Fe/Si ratio, which shows that more amorphous phase is present when more iron is added. CS952 and CS971 follow the same decreasing tendency with increasing Fe/Si. The area is a measure of amorphous phase, consequently the crystallization of the C-S-H gel during autoclaving is equally hindered by iron in the two series.

In **Figure 5-3** BD and CCS as a function of Fe/Si for CS971 and CS952 are shown. It

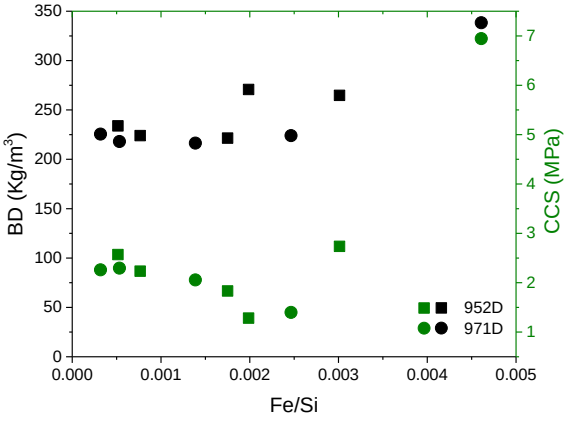

Figure 5-3 *CCS (green) and BD (black) as a function of Fe/Si ratio for CS952 and CS971. Data for CS952 are adapted from Paper II.*

is seen that CCS decreases with increased Fe/Si and then increases at a critical level (Fe/Si ~ 0.0024). The decrease and following increase are very similar for the two types of MS, showing that the iron impact on CCS is the same for both MS types. Further, BD is stable at low Fe/Si, and slightly increases for both MS types as the Fe/Si increases. This shows that the decrease in CCS is not due to lower BD, but due to changes in the structure of the calcium silicate. From both XRD and DSC it is found that with increasing Fe/Si the amorphous phase increases. This indicates that increasing amorphous phase results in lower CCS, until some critical point where the CCS increases. In Chapter 4 CCS is also found to decrease with increasing amorphous phase.

5.2. IRON IMPACT ON CRYSTALLIZATION OF POROUS CALCIUM SILICATES

The crystallization of porous calcium silicates is highly influenced by iron, when added to the MS dispersion before reaction between MS and QL [Paper III]. In the following the influence of iron on the crystallization in the autoclave of calcium silicate is investigated. This is done by adding iron to the C-S-H gel after prereaction.

The production of C-S-H gel follows a standard recipe with Ca/Si molar ratio of 1, produced on the pilot plant using 952D as MS raw material. After prereaction 5 samples are taken from the same reaction slurry, 1 is the reference and to the 4 other samples different concentrations of $Fe(NO_3)_3 \cdot 9H_2O$ are added. The samples are pressed on the small press, which is normally used for laboratory scale samples. After pressing the calcium silicate samples are autoclaved and dried.

The Ca/Si and Fe/Si ratios are determined from XRF results, see **Table 5-2**. The Ca/Si ratio is expected to be the same for all samples, since the samples are made from the same reaction slurry. However, the Ca/Si decreases with higher concentrations of iron added. $Ca(OH)_2$ could react with NO_3 forming $Ca(NO_3)_2$ which has a much higher solubility than $Ca(OH)_2$ [72]. This will result in removal of Ca^{2+} ions during filter pressing of the samples. The Ca/Si ratio is also found to decrease for samples where iron is added before reaction, see **Table 5-1**. This systematic decrease is expected to be caused by the $Ca(NO_3)_2$ formation.

Table 5-2 *Ca/Si and Fe/Si ratios of calcium silicate samples with iron added after prereaction, before autoclaving.*

ID	Ca/Si	Fe/Si
Ref	1.00	0.00050
Fe1	1.00	0.00095
Fe2	0.99	0.00191
Fe3	0.99	0.00340
Fe4	0.97	0.00618

BD, CCS and LS at 950 and 1050 °C are determined for the calcium silicate samples with iron added after prereaction, see **Figure 5-4**. BD is stable for all 5 samples, whereas CCS is found to decrease with increasing Fe/Si. The change in CCS is less when the iron is added after prereaction, compared to when the iron is added during silica dispersion (see **Figure 5-3**, be aware of different scales). LS is found to increase with increasing iron, both at 950 and 1050 °C, where the increase is more pronounced at 1050 °C. Above 1000 °C the iron starts to work as a flux, which results in increased sintering of the material [Paper III].

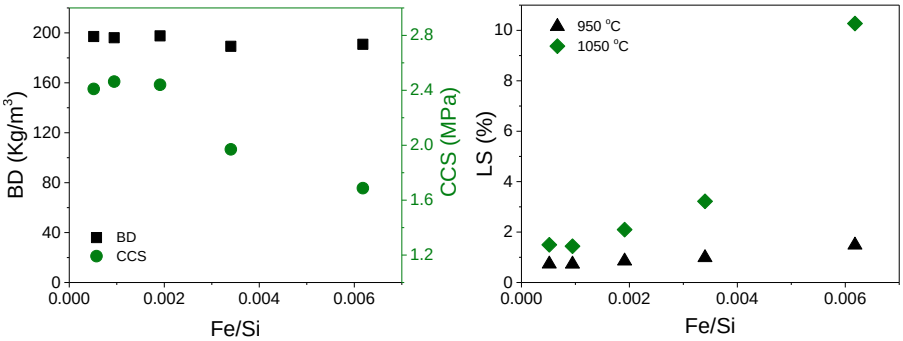

Figure 5-4 *Left: BD and CCS as a function of Fe/Si for calcium silicate with iron added after prereaction. Right: LS at 950 °C and 1050 °C as a function of Fe/Si for calcium silicate with iron added after prereaction.*

The XRD powder patterns of the calcium silicate with iron added after prereaction are seen in **Figure 5-5** together with the XRD powder patterns of calcium silicate with iron added during dispersion of MS. It is seen that the crystal structure is mainly xonotlite at low Fe/Si, but with increasing Fe/Si the xonotlite phase decreases.

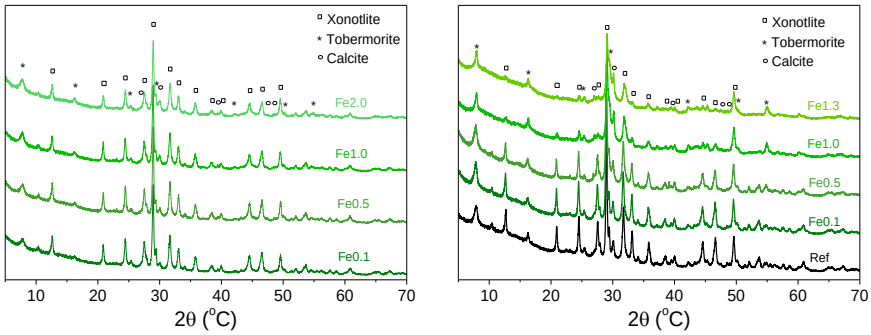

Figure 5-5 *XRD powder patterns of calcium silicate with iron added after prereaction (left) and iron added during dispersion of MS (right). XRD powder pattern for iron added during dispersion of MS is adapted from Paper III.*

The crystal structure of the samples with iron added before prereaction is changing more with increasing Fe/Si, compared to when iron is added after prereaction. This emphasizes, that iron hinders reaction between QL and MS during prereaction [PaperII, PaperIII]. It also shows how important the prereaction is for a well crystallized calcium silicate product as also found in Chapter 1.

The crystal phases are quantified using the Rietveld refinement method and plotted as a function of Fe/Si in **Figure 5-6**. The xonotlite structure decreases with Fe/Si, whereas amorphous phase, tobermorite and calcite phases increase. Xonotlite is important for the thermal stability. The decrease in xonotlite structure with increasing Fe/Si is consistent with the increase in LS at both 950 and 1050 °C. Further the XRD results confirm, that when the amorphous phase increases then the CCS decreases.

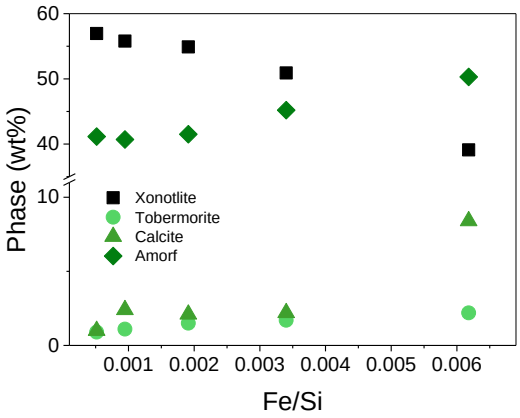

Figure 5-6 *Crystal phases as a function of Fe/Si for calcium silicate with iron added after prereaction. Be aware that the Y-axis is broken between 10 and 35 wt%.*

5.3. SUMMARY

The results show that iron highly impacts the calcium silicate product properties, both when the iron is added before and after prereaction. The impact of iron ions is found to be the same when different MS types are applied in the production of porous calcium silicate.

From the XRD results it is found that iron influences the crystallization of the calcium silicate product, both when the iron is added before and after prereaction. This impact is, however, greatest when the iron is added before prereaction. This shows that iron hinders the polymerization reaction of C-S-H gel. A poorly reacted C-S-H gel results in a poorly crystalized calcium silicate material.

The iron is added as $Fe(NO_3)_3 \cdot 9H_2O$, which is easily soluble in water (82.5 g/100g H_2O [72]), therefore all iron is expected to be accessible for reaction. The impurities present in the MS can be present as metal alloys or oxides, which have a lower solubility than $Fe(NO_3)_3 \cdot 9H_2O$. Therefore, iron present as impurity in the MS is expected to influence the C-S-H gel formation and calcium silicate crystallization differently than shown here.

From these results we can conclude, that it is important to have a low concentration of iron when high temperature stable products are desired. This is important to know, when searching for new raw materials for production of calcium silicate with high temperature stability.

CHAPTER 6. IMPACT OF MICRO SILICA ON POROUS CALCIUM SILICATE PRODUCTS

The calcium silicate product properties are highly dependent on the micro silica (MS) type used as raw material, impurities and processing conditions. This is shown in the previous chapters, where different types of MS are investigated, and different processing conditions are tested. In the following calcium silicate is made in laboratory scale and on the pilot plant with different MS types and discussed together with the results of the previous chapters. The production of the calcium silicate proceeds as described in Section 3.2. 12 MS types are characterized in **Fejl! H envisningskilde ikke fundet.** and 11 of these are made into calcium silicate in laboratory scale. 6 MS types are made into calcium silicate on the pilot plant. The prereaction and autoclave times are fixed, therefore, only differences in reaction rate of the different MS types will influence the product properties.

The crystal phases are detected by XRD and quantified using Rietveld refinement of the calcium silicate samples produced on the pilot plan. The chemical composition is determined with XRF, and from this the Ca/Si molar ratio is determined. In **Figure 6-1** the xonotlite and tobermorite crystal content are plotted as a function of Ca/Si ratio for the calcium silicate samples produced on the pilot plan. It is seen that at low Ca/Si ratio the tobermorite content is high, and as the Ca/Si ratio increases the tobermorite content decreases and the xonotlite content increases.

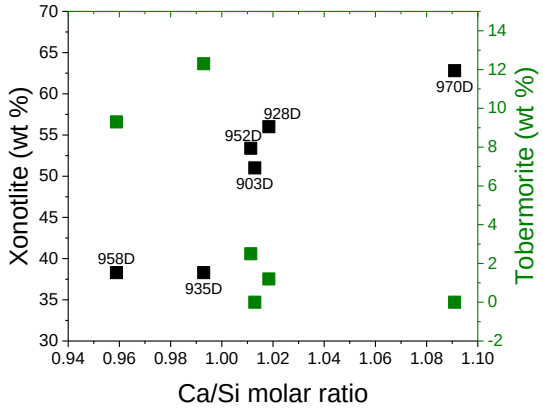

Figure 6-1 *Xonotlite and tobermorite content of 6 calcium silicate samples, with different MS types, produced on the pilot plant, as a function of Ca/Si molar ratio. The prereaction and autoclave times are fixed. Each calcium silicate is marked with the MS type used as raw material.*

In Chapter 1 it is found that the crystal content is dependent on autoclave time and reaction time. Therefore, a well reacted C-S-H gel is expected to result in a high degree of crystallinity. Hence, the crystal structure is also dependent on the degree of reaction, and not only Ca/Si ratio. A well reacted C-S-H gel results in a low bulk density (BD), since the highly polymerized C-S-H gel network will result in increased porosity of the material, see Chapter 1 and ref. [1]. The dissolution of the MS particles is expected to be the rate determining factor, therefore, the MS particle size should influence the conversion rate.

In **Figure 6-2** (left) BD of the calcium silicate samples produced on the pilot plant is plotted as a function of the MS particle size. From the figure it is found, that a small particle size results in low density, i.e. well-reacted C-S-H gel. This corresponds with the findings of Greenberg [4], who found that the larger the surface area, the higher the reaction rate. Impurities also influence the reaction between MS and QL [PaperII]. The electrical conductivity of the dispersed MS suspension gives an indication of the amount of impurities available during prereaction. In **Figure 6-2** (right) BD of the different calcium silicate samples is plotted as a function of the electrical conductivity of suspended MS, used as raw material. There is a tendency for BD to increase as the electrical conductivity increases. This indicates that the dissolved impurities from the MS influence the reaction rate, which confirm that impurities influence the reaction between MS and QL [Paper II].

In **Figure 6-2** calcium silicate made with 952D is found to deviate from the other calcium silicate samples regarding BD as a function of both particle size and electrical conductivity. This indicates that a third factor influences the reaction between MS and QL. It is suggested that a high number of surface hydroxyl groups will result in a faster reaction between MS and QL, compared to a low number of surface hydroxyl groups

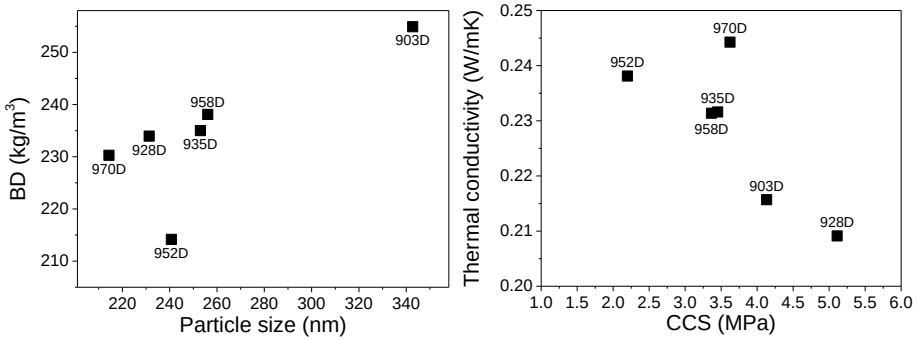

Figure 6-2 *Bulk density (BD) of calcium silicate samples produced on the pilot plant with 6 different types of MS. BD is plotted as a function of particle size (left) and as a function of electrical conductivity (right). Particle size and electrical conductivity is determined on the 6 different types of MS dispersed in water. Each calcium silicate is marked with the MS used as raw material.*

[PaperIV]. If 952D has a higher number of surface hydroxyl groups than any of the other MS tested, then a higher reaction rate is expected.

From the laboratory scale samples, the correlation of CCS with BD and amorphous phase is determined. The amorphous phase is determined from XRD, using the Rietveld refinement method with external standard. In **Figure 6-3** CCS as a function of BD (left) and amorphous phase (right) are plotted of the laboratory scale calcium silicates. It is seen that CCS as a function of BD decreases, which is opposite to the results in **Figure 4-1**, where CCS increases when BD increases. From **Figure 6-3** (right) it is found that CCS as a function of amorphous phase decreases. This corresponds with previous results in both Chapter 1 and 0, where low crystalline content results in low CCS. This indicates that the decrease in CCS with BD is due to the difference in crystal phase and that the crystal structure of the material has a higher impact on CCS than BD does, in the BD range tested.

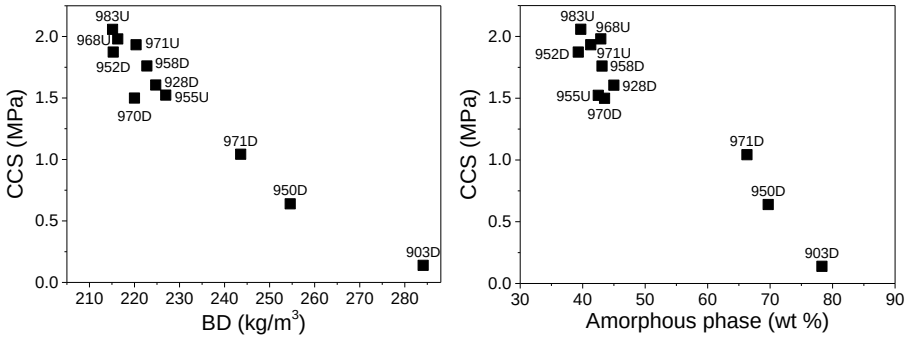

Figure 6-3 *CCS as a function of BD (left) and amorphous phase (right) for laboratory scale calcium silicate produced with different types of MS.*

The chemical bonding of laboratory scale calcium silicate produced with different MS types is investigated using Fourier transform infrared spectroscopy (FTIR) as shown in **Figure 6-4**. Only 9 samples are shown in **Figure 6-4**, due to the similarity of 928D and 952D with 983U, 971U and 970U.

At 3640 cm^{-1} the CaO-H stretching mode in xonotlite is found. The CaO-H bonds are only present in xonotlite and not in tobermorite [56], however, no band is found at 3640 cm^{-1} for calcium silicate made with 903D, 950D and 971D as raw materials. At 1204 cm^{-1} a clear band is seen, this band is due to Si-O stretching vibrations in Q^3 sites [52]. Q^3 sites are also present in the xonotlite crystal [60] and is also an indication of increased polymerization [1]. This indicates that no xonotlite is formed in samples with 903D, 950D and 971D as raw material and that poor C-S-H gel is formed in the prereaction of these samples [Paper III]. All samples have an intense band in the range from 1000-950 cm^{-1}, attributed to the Si-O stretching vibrations in Q^2 sites. This band is less intense for samples with 903D, 950D and 971D as raw material.

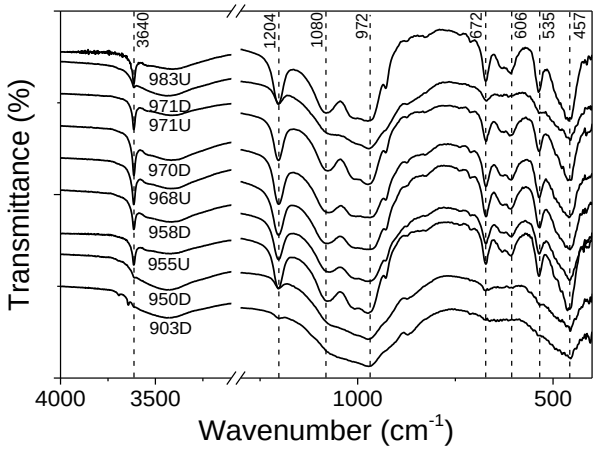

Figure 6-4 *FTIR of laboratory scale calcium silicate samples prepared with different types of MS. The y-axis is shifted vertically for clarity.*

In Paper II and Chapter 1 it is found that different MS react differently and that increased reaction time results in increased C-S-H gel formation and increased crystal formation. In **Figure 6-4** it is found that the C-S-H gel formation is different among the calcium silicate samples produced with different MS types. This indicates that the reaction rate of the different MS types is different. Amorphous phase and CCS are found to be low for samples with 971D, 950D and 903D, which are also the samples with poor C-S-H gel found from FTIR results. All these factors indicate that 903D, 950D and 971D react slower than the remaining MS types.

The MS-QL reaction is highly dependent on well dispersed MS particles. Densified MS particles are generally more difficult to disperse than undensified, see **Figure 2-8.** In **Figure 6-3** the three samples with lowest CCS are all produced with densified MS as raw material. It is possible that the MS is not properly dispersed before reaction, leading to slower reaction. The particle size of the different MS types is determined and found in **Table 2-2**, however, no correlation is found between particle size and amount of amorphous phase or CCS for calcium silicate produced in laboratory scale. It is possible that some of the MS are insufficiently dispersed prior to prereaction, but it can also be due to variation in impurity content. In Paper II it is found that impurities influence the reaction rate between MS and QL and in Paper III it is found, that iron highly impacts the reaction between QL and MS when present as ions. In Section 5.2 it is shown that the iron also impacts the crystal formation in the autoclave. 903D shows the poorest C-S-H gel and crystal formation and is the MS with the highest impurity content and display a large particle size. The remaining 10 calcium silicate samples prepared with different types of MS in laboratory scale show no correlation with amorphous content and different types of impurities. This shows that the impurity impact is very complicated, and most likely depend on the impurity types and how the impurities are present. The amorphous phase is also related to the reaction rate,

therefore, the MS impact on calcium silicate is likely to be an effect of both particle size, impurities and surface hydroxyl groups.

6.1. IMPURITY IMPACT ON POROUS CALCIUM SILICATES

The chemical composition of the calcium silicate samples is determined with XRF for both laboratory scale and pilot plant samples. The impurity impact on linear shrinkage (LS) is illustrated in **Figure 6-5**, where LS is plotted as a function of Fe/Si molar ratio (left) and total metallic impurities in wt % (M total). It is found that LS increases as Fe/Si molar ratio increases, which is also found in Paper III. In Paper III only Fe is investigated, but in **Figure 6-5** (right) the impact of total metallic impurities is shown. The results indicate that impurities generally influence LS. The impact is especially seen at high temperatures, where the material starts to sinter.

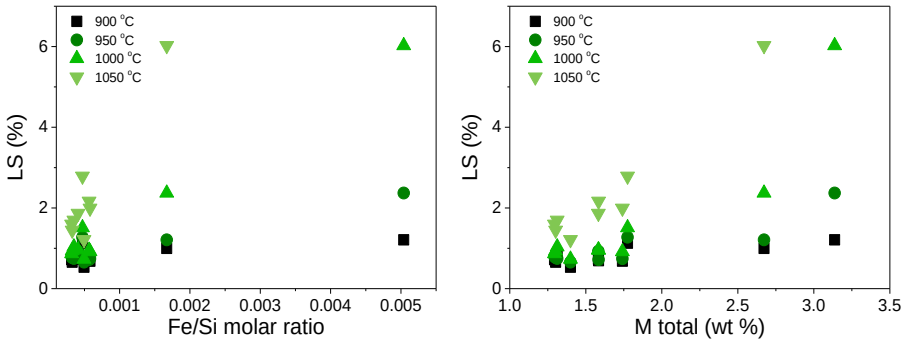

Figure 6-5 *Linear shrinkage (LS) as a function of Fe/Si molar ratio (left) and total metallic impurities (right) in calcium silicate samples produced with different MS types in laboratory scale.*

LS is also determined at 950 and 1050 °C for the pilot plant calcium silicate samples prepared with 6 different MS types, and in **Figure 6-6** LS as a function of total metallic impurities is plotted. As the impurity level increases in the different calcium silicate samples the LS also increases. This again confirms that impurities influence the thermal stability of the calcium silicate material.

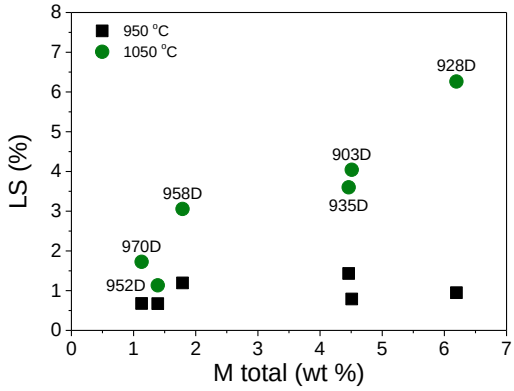

Figure 6-6 *Linear shrinkage (LS) at 950 and 1050 °C as a function of total metallic impurities (M total) for calcium silicate produced with 6 different MS types on the pilot plant. The calcium silicate samples are marked with the MS type used as raw material.*

6.2. THERMAL CONDUCTIVITY OF POROUS CALCIUM SILICATES

The thermal conductivity of the calcium silicate samples produced on the pilot plant is measured with the hot disc method (Hot Disc TPS2500, Sweden) [73]. The thermal conductivity is measured first at 23 ± 1 °C and then at 700, 500 and 200 °C, see **Figure 6-7**. The measurement is held at 700 °C for 1 hour before the measurement starts. During this time all organic fibers are oxidized and the phase transition from tobermorite and xonotlite to wollastonite starts. Therefore, samples measured at 700, 500 and 200 °C are mainly wollastonite.

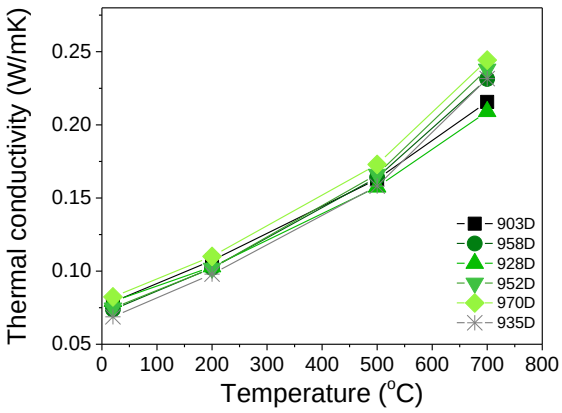

Figure 6-7 *Thermal conductivity as a function of temperature for calcium silicate produced with different types of micro silica.*

The thermal conductivity increases as the temperature rises. The increase in thermal conductivity with temperature varies within the different samples. At 20 °C the thermal conductivity is lowest for calcium silicate produced with 935D, however, at 700 °C the lowest thermal conductivity is obtained for the sample produced with 928D. The thermal conductivity is related to the porosity of the material, where a high porosity (or a low BD) results in low thermal conductivity [74]. In **Figure 6-8** the thermal conductivity determined at 20 and 700 °C is plotted as a function of BD. However, no correlation is found between thermal conductivity and BD both at 20 and 700 °C. This indicates that other factors also influence the thermal conductivity of porous calcium silicate materials.

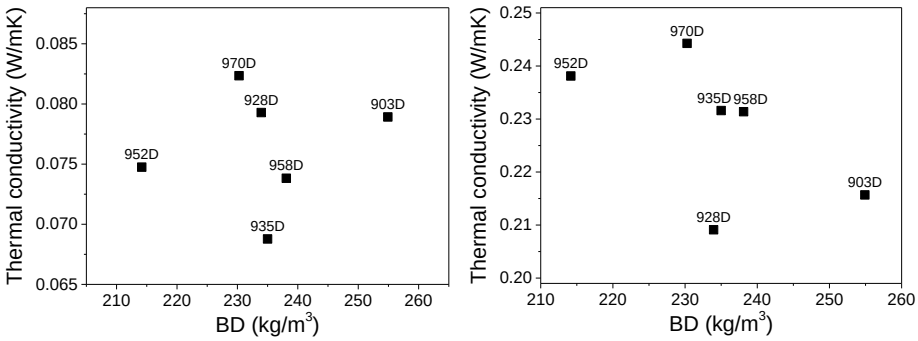

Figure 6-8 *Thermal conductivity as a function of bulk density (BD). The thermal conductivity is measured at 20 °C (left) and at 700 °C (right).*

For porous insulating materials the heat transfer mechanism is influenced by conduction and radiation. Convection can be neglected when the pores are < 4 mm [75], which is the case for porous calcium silicates. At low temperatures conduction is the main mechanism of heat transfer and as the temperature increases radiation becomes dominant [76]. Conduction is the movement of phonons in the material and is influenced by the material structure [77]. In amorphous materials the free pathlength is short and the movement of phonons are hindered. In crystals the phonons can move in the crystal lattice, which results in high thermal conductivity at low temperatures, and decreases with increased temperature due to thermal motion. As the temperature increases the crystal lattice becomes less perfect and the free pathway of the phonons become shorter. In materials the thermal conductivity is influenced by the number of grain boundaries that hinders the phonon movement. A high number of small crystallites will result in a low thermal conductivity due to scattering of phonons, compared to a low number of larger crystallites [74].

It is expected that the thermal conductivity will be low with a high amorphous content at 20 °C, due to the short pathlength of phonons in amorphous materials. In **Figure 6-9** the thermal conductivity as a function of amorphous phase at 20 °C (left) is plotted for calcium silicate with 6 different types of MS produced on the pilot plant. There is a weak tendency for the thermal conductivity to decrease as the amorphous phase

increases. The thermal conductivity of calcium silicate produced with 903D is high compared to the high amorphous content. This could be due to the higher BD of this sample, see **Figure 6-8**. The thermal conductivity of calcium silicate with 935D is lower than the general trend. This can be due to the high tobermorite content in this sample, compared to tobermorite content of the remaining samples. Tobermorite is generally more disordered than xonotlite and should therefore result in a lower thermal conductivity. The results at 20 °C show that bulk density, amorphous content and type of crystal phase all influence the thermal conductivity of porous calcium silicates.

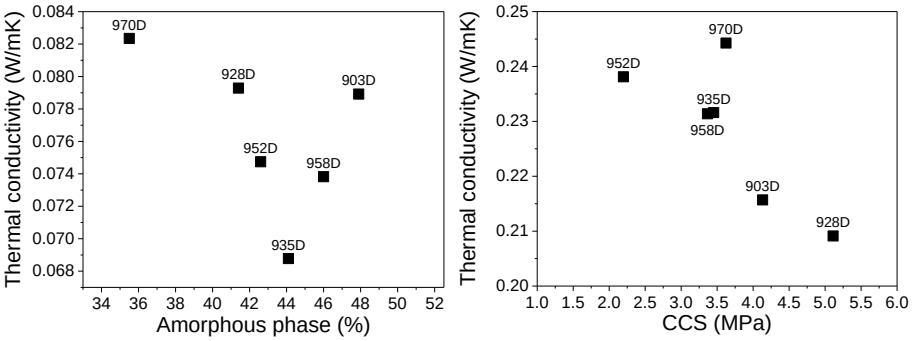

Figure 6-9 *Left: thermal conductivity at 20 °C as a function of amorphous phase. Right: thermal conductivity at 700 °C as a function of cold compressive strength (CCS).*

In **Figure 6-9** (right) the thermal conductivity measured at 700 °C as a function of CCS is plotted for calcium silicate produced with 6 different types of MS on the pilot plant. It is found that at high CCS a low thermal conductivity at 700 °C is obtained. A low thermal conductivity is obtained with a high number of small crystallites. Since CCS is high at low thermal conductivity, the results indicate that a high number of small crystallites also result in high CCS. The thermal conductivity of 970D has a high thermal conductivity at high CCS compared to the other samples. Calcium silicate produced with 970D is also the sample with highest crystalline content, see **Figure 6-1**. The high thermal conductivity can be explained by the presence of large crystals with less contact points, that increases the thermal conductance in the material. The correlation between CCS and thermal conductivity show that CCS is not only dependent of high crystal content and BD, but also on the size of the crystallites.

6.3. SUMMARY

Properties of calcium silicate are dependent on the characteristics of the MS used as raw material. Particle size and impurities are found to influence the reaction rate of MS. A fast reaction rate is important to obtain high crystal content and high cold

compressive strength. A low degree of impurities is important for high thermal stability.

Calcium silicate is applied in both high temperature industries and buildings. Depending on where the material is applied different product properties are important.

Applications in buildings require low thermal conductivity. Low thermal conductivity at room temperature is obtained with high amorphous phase, high tobermorite content and low bulk density. A low bulk density is obtained by a fast reacting MS or long reaction time. This generally leads to increased crystal formation especially xonotlite, which is not desired for low thermal conductivity. A high tobermorite content leads to lower thermal conductivity than xonotlite does. To obtain higher tobermorite content the Ca/Si ratio should be below 1.

For high temperature industries high thermal stability, high cold compressive strength and low thermal conductivity are important properties. To obtain high thermal stability it is important with low impurity content and a high xonotlite content. The high strength and low thermal conductivity is obtained with a high number of small crystals.

CHAPTER 7. CONCLUSIONS AND PERSPECTIVES

Porous calcium silicate samples with different types of micro silica as raw material are produced to investigate the impact of micro silica on the calcium silicate product properties.

Micro silica types from different suppliers are characterized as-received and dispersed in water. The chemical composition, crystalline impurities and crystallization temperature of the as received micro silica are different among different micro silica types. The crystallization temperature is not only dependent on chemical and crystalline impurities, but also whether the impurities are present as impurity particles among micro silica particles, on the surface of the micro silica particles and on the distribution of impurities. The particle size, zeta potential and electrical conductivity of micro silica dispersed in water are also different among different micro silica types. The dissolved impurities contributing to electrical conductivity are also found to lower crystallization temperature. Therefore, the electrical conductivity provides an indicator of the crystallization temperature of micro silica.

Reaction and autoclave time highly impact the porous calcium silicate product properties. Increased reaction time results in low bulk density and increased xonotlite content in the autoclave. Increased autoclave time leads to increased crystal formation, especially the formation of xonotlite increases.

The crystal phase and amount of crystal influence cold compressive strength, linear shrinkage and thermal conductivity of the calcium silicate material. The thermal conductivity at 700 °C is related to cold compressive strength. A low thermal conductivity is obtained with a high number of crystallites, which is found to result in high cold compressive strength. Cold compressive strength is related to the bulk density and amount of crystal in the calcium silicate material. The correlation between cold compressive strength and bulk density of porous calcium silicates differ when various types of micro silica are used as raw material. This difference in correlation of cold compressive strength and bulk density for porous calcium silicate with different micro silica types is not determined. An improved understanding of the nucleation and crystallization in the calcium silicate material is of interest, to be able to design materials with higher strength and lower thermal conductivity.

Thermal conductivity at room temperature is lowest with low bulk density and high amorphous and tobermorite phase. The amorphous phase can be controlled by decreasing the autoclave time and the tobermorite content can be increased by lowering the Ca/Si ratio to 0.83.

The surface hydroxyl groups of micro silica are expected to influence the reaction rate. This is, however, not thoroughly investigated in this work, though it would be of great interest to get a deeper understanding of the impact of surface hydroxyl groups on the reaction rate between micro silica and quicklime.

Impurities are always present in micro silica due to the production method. The impurities work as fluxes in the calcium silicate, hence lowering the thermal stability of the calcium silicate product. Products that require high thermal stability (above ~1000 °C) can only be produced with high purity micro silica with SiO_2 content above ~95 wt%. Among the impurities, iron is shown to inhibit the C-S-H gel and xonotlite formation when present as ions. This results in low cold compressive strength and low thermal stability. It is of interest to investigate whether an additive can be added during calcium silicate production, which can shield the negative effects of iron and other impurities. This is of interest, since micro silica types with high SiO_2 content generally are more expensive than micro silica with low SiO_2 content.

Based on a deeper understanding of the reaction and processing conditions of porous calcium silicate, the criteria of micro silica for producing calcium silicate boards with low bulk density, low thermal conductivity, high strength and high thermal stability can be specified. The criteria for micro silica are small particle size, low impurity content and a high number of surface hydroxyl groups. However, micro silica is a by-product and the properties are rarely designed to have a specific particle size, impurity content or surface hydroxyl groups. Instead the prereaction time of calcium silicate should be optimized to obtain the same calcium silicate product properties with different types of micro silica.

BIBLIOGRAPHY

[1] H.-I. Hsiang, W.-S. Chen, W.-C. Huang, Pre-reaction temperature effect on C–S–H colloidal properties and xonotlite formation via steam assisted crystallization, Mater. Struct. 49 (2016) 905–915. doi:10.1617/s11527-015-0547-0.

[2] W. Nocun-Wczelik, Effect of some inorganic admixtures on the formation and properties of calcium silicate hydrates produced in hydrothermal conditions, Cem. Concr. Res. 27 (1997) 83–92.

[3] S. Shaw, S. Clark, C.M.. Henderson, Hydrothermal formation of the calcium silicate hydrates, tobermorite (Ca5Si6O16(OH)2 4H2O) and xonotlite (Ca6Si6O17(OH)2): an in situ synchrotron study, Chem. Geol. 167 (2000) 129–140.

[4] S.A. Greenberg, Reaction between Silica and Calcium Hydroxide Solutions. I. Kinetics in the Temperature Range 30 to 85, J. Phys. Chem. 65 (1961) 12–16. http://pubs.acs.org/doi/pdf/10.1021/j100819a005.

[5] K. Matsui, J. Kikuma, M. Tsunashima, T. Ishikawa, S.Y. Matsuno, A. Ogawa, et al., In situ time-resolved X-ray diffraction of tobermorite formation in autoclaved aerated concrete: Influence of silica source reactivity and Al addition, Cem. Concr. Res. 41 (2011) 510–519. doi:10.1016/j.cemconres.2011.01.022.

[6] I. Pignatelli, A. Kumar, M. Bauchy, G. Sant, Topological control on silicates' dissolution kinetics, Langmuir. 32 (2016) 4434–4439. doi:10.1021/acs.langmuir.6b00359.

[7] S. Bai, H. Mu, G. Naren, Y. Okaue, T. Yokoyama, Kinetic study of silica dissolution in aqueous solutions of aromatic organic electrolytes, Colloids Surfaces A Physicochem. Eng. Asp. 461 (2014) 220–224. doi:10.1016/j.colsurfa.2014.07.048.

[8] M. Bauchy, M.J.A. Qomi, F.J. Ulm, R.J.M. Pellenq, Order and disorder in calcium-silicate-hydrate, J. Chem. Phys. 140 (2014). doi:10.1063/1.4878656.

[9] F.P. Glasser, S.Y. Hong, Thermal treatment of C-S-H gel at 1 bar H2O pressure up to 200°C, Cem. Concr. Res. 33 (2003) 271–279. doi:10.1016/S0008-8846(02)00959-6.

[10] A. Moropoulou, A. Bakolas, E. Aggelakopoulou, The effects of limestone characteristic, granulation and calcination temperature to the reactivity of

quicklime, Cem. Concr. Res. 31 (2001) 633–639. doi:10.1016/S0008-8846(00)00490-7.

[11] D.T. Beruto, R. Botter, R. Cabella, A. Lagazzo, A consecutive decomposition-sintering dilatometer method to study the effect of limestone impurities on lime microstructure and its water reactivity, J. Eur. Ceram. Soc. 30 (2010) 1277–1286. doi:10.1016/j.jeurceramsoc.2009.12.012.

[12] G. Leontakianakos, I. Baziotis, A. Papandreou, D. Kanellopoulou, V.N. Stathopoulos, S. Tsimas, A comparative study of the physicochemical properties of Mg-rich and Ca-rich quicklimes and their effect on reactivity, Mater. Struct. 48 (2015) 3735–3753. doi:10.1617/s11527-014-0436-y.

[13] T. Oates, Kirk-Othmer Encyclopedia of Chemical Technology, in: Kirk-Othmer Encycl. Chem. Technol., John Wiley & Sons, Inc., Hoboken, NJ, USA, 2010. doi:10.1002/0471238961.1209130507212019.a01.pub3.

[14] J.-M. Commandre, S. Salvador, A. Nzihou, REACTIVITY OF LABORATORY AND INDUSTRIAL LIMES, Chem. Eng. Res. Des. 85 (2007) 473–480. doi:10.1205/cherd06200.

[15] R.H. Borgwardt, Calcination kinetics and surface area of dispersed limestone particles, AIChE J. 31 (1985) 103–111. doi:10.1002/aic.690310112.

[16] J.M. Valverde, P.E. Sanchez-Jimenez, L.A. Perez-Maqueda, Limestone calcination nearby equilibrium: Kinetics, CaO crystal structure, sintering and reactivity, J. Phys. Chem. C. 119 (2015) 1623–1641. doi:10.1021/jp508745u.

[17] B. V. L'vov, L.K. Polzik, V.L. Ugolkov, Decomposition kinetics of calcite: a new approach to the old problem, Thermochim. Acta. 390 (2002) 5–19. doi:10.1016/S0040-6031(02)00080-1.

[18] A.A. Matvienko, S.A. Chizhik, A.A. Sidel'nikov, A new kinetic model of calcite thermal decomposition, Dokl. Phys. Chem. 451 (2013) 647–649. doi:10.1134/S001250161308006X.

[19] E.L. Fuller, T.R. Yoos, Surface Properties of Limestones and Their Activation Products, Langmuir. 3 (1987) 753–760. doi:10.1021/la00077a032.

[20] H. Shi, Y. Zhao, W. Li, Effects of temperature on the hydration characteristics of free lime, Cem. Concr. Res. 32 (2002) 789–793. doi:10.1016/S0008-8846(02)00714-7.

[21] J. Tang, R. Guo, J. Wang, Inhibition of interaction between kaolinite and K 2

CO 3 by pretreatment using calcium additive, J. Therm. Anal. Calorim. 114 (2013) 153–160. doi:10.1007/s10973-012-2905-2.

[22] L. Desgranges, D. Grebille, G. Calvarin, G. Chevrier, N. Floquet, J.-C. Niepce, Hydrogen thermal motion in calcium hydroxide: Ca(OH)2, Acta Crystallogr. Sect. B Struct. Sci. 49 (1993) 812–817. doi:10.1107/S0108768193003556.

[23] E.D. Rodríguez, L. Soriano, J. Payá, M.V. Borrachero, J.M. Monzó, Increase of the reactivity of densified silica fume by sonication treatment, Ultrason. Sonochem. 19 (2012) 1099–1107. doi:10.1016/j.ultsonch.2012.01.011.

[24] S. Goberis, V. Antonovich, I. Pundene, R. Stonis, Effect of the quality of microsilica on the flow properties of cement slurry and characteristics of low-cement refractory concrete on a chamotte filler, Refract. Ind. Ceram. 48 (2007) 123–127. doi:10.1007/s11148-007-0042-4.

[25] S. Diamond, S. Sahu, Densified silica fume: particle sizes and dispersion in concrete, Mater. Struct. 39 (2006) 849–859. doi:10.1617/s11527-006-9087-y.

[26] R. Lamy, E. Zunic, R. Steding, A. Aamodt, Preparation of stable slurries of spherically shaped silica for coatings, Prog. Org. Coatings. 72 (2011) 96–101. doi:10.1016/j.porgcoat.2011.03.020.

[27] B. Schickle, R. Telle, T. Tonnesen, C. Frederik, A. Opsommer, Factors of Influence on the Crystallisation of Calcium Silicates Under Hydrothermal Conditions and the Effecting Thermal Stability at Higher Temperatures, in: 54th Int. Colloq. Refract. 2011 - Refract. Ind., Aachen, 2011: pp. 61–64.

[28] M. Bruno, J.L. Holm, An investigation of microsilica by thermoanalytical methods, Thermochim. Acta. 318 (1998) 125–129. doi:10.1016/S0040-6031(98)00336-0.

[29] G.-W. Lask, Fremgangsmåde til fremstilling af silicium i en elektroovn ud fra kvarts og carbon, DK382981A, 1981.

[30] K. Heggestad, J.L. Holm, K. Lønvik, B. Sandberg, Investigations of Elkem Micro Silica by thermosonimetry, Thermochim. Acta. 72 (1984) 205–212. doi:10.1016/0040-6031(84)85075-3.

[31] W. Zhu, Y. Zhou, W. Ma, M. Li, J. Yu, K. Xie, Using silica fume as silica source for synthesizing spherical ordered mesoporous silica, Mater. Lett. 92 (2013) 129–131. doi:10.1016/j.matlet.2012.10.044.

[32] A. Hamoudi, L. Khouchaf, C. Depecker, B. Revel, L. Montagne, P. Cordier, Microstructural evolution of amorphous silica following alkali – silica reaction, J. Non. Cryst. Solids. 354 (2008) 5074–5078. doi:10.1016/j.jnoncrysol.2008.07.001.

[33] F. Meneau, G.N. Greaves, R. Winter, Y. Vaills, WAXS and NMR studies of intermediate and short range order in K2O-SiO2 glasses, J. Non. Cryst. Solids. 293–295 (2001) 693–699. doi:10.1016/S0022-3093(01)00848-1.

[34] L. Armelao, M. Fabrizio, S. Gross, A. Martucci, E. Tondello, Molecularly interconnected SiO2–GeO2 thin films: sol–gel synthesis and characterization, J. Mater. Chem. 10 (2000) 1147–1150. doi:10.1039/a907247k.

[35] N. Marinoni, M.A.T.M. Broekmans, Microstructure of selected aggregate quartz by XRD, and a critical review of the crystallinity index, Cem. Concr. Res. 54 (2013) 215–225. doi:10.1016/j.cemconres.2013.08.007.

[36] Y.Z. Yue, Anomalous Enthalpy Relaxation in Vitreous Silica, Front. Mater. 2 (2015) 1–11. doi:10.3389/fmats.2015.00054.

[37] M. Jensen, R. Keding, T. Höche, Y.Z. Yue, Biologically Formed Mesoporous Amorphous Silica, J. Am. Chem. Soc. 131 (2009) 2717–2721. doi:10.1021/ja808847y.

[38] S. Liu, H. Tao, Y. Zhang, Y.Z. Yue, Reduction-Induced Inward Diffusion and Crystal Growth on the Surfaces of Iron-Bearing Silicate Glasses, J. Am. Ceram. Soc. 98 (2015) 1799–1806. doi:10.1111/jace.13587.

[39] R.K. Iler, The Chemistry of Silica: Solubility, Polymerization, Colloid and Surface Properties and Biochemistry of Silica, John Wiley, New York, 1979.

[40] P.J. Lezzi, E.E. Evke, E.M. Aaldenberg, M. Tomozawa, Surface Crystallization and Water Diffusion of Silica Glass Fibers : Causes of Mechanicl Strnegth Degradtion, J. Am. Ceram. Soc. 11 (2015) 1–11. doi:10.1111/jace.13597.

[41] O.A. Alharbi, D.Y. Zaki, E.M.A. Hamzawy, Effect of TiO2, LiF and Cr2O3 in the Crystallization of Cristobalite and Tridymite in Sintered Glass-Ceramics, Silicon. 4 (2012) 281–287. doi:10.1007/s12633-012-9132-0.

[42] A. Kerrache, V. Teboul, A. Monteil, Screening dependence of the dynamical and structural properties of BKS silica, Chem. Phys. 321 (2006) 69–74. doi:10.1016/j.chemphys.2005.07.039.

[43] J.E. Shelby, Introduction to glass science and technology, Royal Society of Chemistry, 2005.

[44] S. Cerveny, G.A. Schwartz, J. Otegui, J. Colmenero, J. Loichen, S. Westermann, Dielectric Study of Hydration Water in Silica Nanoparticles, J. Phys. Chem. C. 116 (2012) 24340–24349. doi:10.1021/jp307826s.

[45] S.K. Milonjić, L.S. Cerović, D.M. Cokesa, S. Zec, The influence of cationic impurities in silica on its crystallization and point of zero charge., J. Colloid Interface Sci. 309 (2007) 155–159. doi:10.1016/j.jcis.2006.12.033.

[46] T. Oertel, F. Hutter, U. Helbig, G. Sextl, Amorphous silica in ultra-high performance concrete : First hour of hydration, Cem. Concr. Res. 58 (2014) 131–142. doi:10.1016/j.cemconres.2014.01.008.

[47] S. Srinivasan, S.A. Barbhuiya, D. Charan, S.P. Pandey, Characterising cement-superplasticiser interaction using zeta potential measurements, Constr. Build. Mater. 24 (2010) 2517–2521. doi:10.1016/j.conbuildmat.2010.06.005.

[48] M.E. Binkley, Method of manufacture of heat insulating shapes, US2699097, 1953.

[49] S. Grangeon, F. Claret, Y. Linard, C. Chiaberge, X-ray diffraction: A powerful tool to probe and understand the structure of nanocrystalline calcium silicate hydrates, Acta Crystallogr. Sect. B Struct. Sci. Cryst. Eng. Mater. 69 (2013) 465–473. doi:10.1107/S2052519213021155.

[50] H.F.W. Taylor, Proposed Structure for Calcium Silicate Hydrate Gel, J. Am. Ceram. Soc. 69 (1986) 464–467. doi:10.1111/j.1151-2916.1986.tb07446.x.

[51] M. Monasterio, J.J. Gaitero, E. Erkizia, A.M. Guerrero, L.A. Miccio, J.S. Dolado, et al., Effect of addition of silica- and amine functionalized silica-nanoparticles on the microstructure of calcium silicate hydrate (C – S – H) gel, J. Colloid Interface Sci. 450 (2015) 109–118. doi:10.1016/j.jcis.2015.02.066.

[52] P. Yu, R.J. Kirkpatrick, B. Poe, P.F. McMillan, X. Cong, Structure of Calcium Silicate Hydrate (C-S-H): Near-, Mid-, and Far-Infrared Spectroscopy, J. Am. Ceram. Soc. 82 (1999) 742–748. doi:10.1111/j.1151-2916.1999.tb01826.x.

[53] F. Battocchio, P.J.M. Monteiro, H.R. Wenk, Rietveld refinement of the structures of 1.0 C-S-H and 1.5 C-S-H, Cem. Concr. Res. 42 (2012) 1534–1548. doi:10.1016/j.cemconres.2012.07.005.

[54] X. Cong, R.J. Kirkpatrick, 29Si and 17O NMR investigation of the structure of some crystalline calcium silicate hydrates, Adv. Cem. Based Mater. 3 (1996) 133–143. doi:10.1016/S1065-7355(96)90045-0.

[55] X. Yang, C. Cui, X. Cui, G. Tang, H. Ma, High-temperature Phase Transition and the Activity of Tobermorite, J. Wuhan Univ. Technol. Sci. Ed. 29 (2013) 298–301. doi:10.1007/s11595-014-0911-x.

[56] N.Y. Mostafa, A.A. Shaltout, H. Omar, S.A. Abo-El-Enein, Hydrothermal synthesis and characterization of aluminium and sulfate substituted 1.1 nm tobermorites, J. Alloys Compd. 467 (2009) 332–337. doi:10.1016/j.jallcom.2007.11.130.

[57] S. Grangeon, A. Fernandez-Martinez, A. Baronnet, N. Marty, A. Poulain, E. Elkaïm, et al., Quantitative X-ray pair distribution function analysis of nanocrystalline calcium silicate hydrates: A contribution to the understanding of cement chemistry, J. Appl. Crystallogr. 50 (2017) 14–21. doi:10.1107/S1600576716017404.

[58] M.J. Abdolhosseini Qomi, K.J. Krakowiak, M. Bauchy, K.L. Stewart, R. Shahsavari, D. Jagannathan, et al., Combinatorial molecular optimization of cement hydrates, Nat. Commun. 5 (2014) 1–10. doi:10.1038/ncomms5960.

[59] F. Liu, L. Zeng, J. Cao, J. Li, Preparation of ultra-light xonotlite thermal insulation material using carbide slag, J. Wuhan Univ. Technol. Mater. Sci. Ed. 25 (2010) 295–297. doi:10.1007/s11595-010-2295-x.

[60] S. V. Churakov, P. Mandaliev, Structure of the hydrogen bonds and silica defects in the tetrahedral double chain of xonotlite, Cem. Concr. Res. 38 (2008) 300–311. doi:10.1016/j.cemconres.2007.09.014.

[61] W. Nocun-Wczelik, Effect of Na and Al on the phase composition and morphology of autoclaved calcium silicate hydrates, Cem. Concr. Res. 29 (1999) 1759–1767. doi:10.1016/S0008-8846(99)00166-0.

[62] K. Baltakys, E. Prichockiene, Influence of CaO reactivity on the formation of low-base calcium silicate hydrates, Mater. Sci. 28 (2010) 295–304.

[63] T. Mitsuda, J. Saito, E. Hattor, Influence of starting materials on the hydrothermal formation of xonotlite at 180C, in: Symp. First Int. Symp. Hydrothermal React., 1983: pp. 823–837.

[64] S. Shaw, C.M.B. Henderson, B.U. Komanschek, Dehydration/ recrystallization mechanisms, energetics, and kinetics of hydrated calcium

silicate minerals: An in situ TGA/DSC and synchrotron radiation SAXS/WAXS study, Chem. Geol. 167 (2000) 141–159. doi:10.1016/S0009-2541(99)00206-5.

[65] E. Spudulis, V. Šavareika, A. Špokauskas, Influence of Hydrothermal Synthesis Condition on Xonotlite Crystal Morphology, Mater. Sci. 19 (2013) 190–196.

[66] S.A. Hamid, The crystal structure of the 11 Å natural tobermorite Ca2.25[Si3O7.5(OH)1.5]·1H2O, Zeitschrift Für Krist. - Cryst. Mater. 154 (1981) 189–198. doi:10.1524/zkri.1981.154.14.189.

[67] H. Chessin, W.C. Hamilton, B. Post, Position and thermal parameters of oxygen atoms in calcite, Acta Crystallogr. 18 (1965) 689–693. doi:10.1107/S0365110X65001585.

[68] L. Galvánková, J.Ĝ. Másilko, T. Solný, E.Š. Č, Tobermorite synthesis under hydrothermal conditions, Procedia Eng. 151 (2016) 100–107. doi:10.1016/j.proeng.2016.07.394.

[69] S.A.S. El-Hemaly, T. Mitsuda, H.F.W. Taylor, Synthesis of normal and anomalous tobermorites, Cem. Concr. Res. 7 (1977) 429–438.

[70] B. Zelinski, D. Uhlmann, Gel technology in ceramics, J. Phys. Chem. Solids. 45 (1984) 1069–1090. doi:10.1016/0022-3697(84)90049-0.

[71] C.-J. Ke, B. Yuan, H. Wang, W.-Z. Wu, Influence of Different Ions for Hydrated Calcium Silicates Under Autoclaved Condition, in: Proc. 11th Int. Symp. Struct. Eng. Vol I II, Science press Beijing, 2010: pp. 1743–1748.

[72] J.R. Rumble, ed., CRC handbook of chemistry and physics : a ready-reference book of chemical and physical data, 98th ed., CRC Press/Taylor & Francis, Boca Raton, 2018.

[73] S.E. Gustafsson, Transient plane source techniques for thermal conductivity and thermal diffusivity measurements of solid materials, Rev. Sci. Instrum. 62 (1991) 797–804. doi:10.1063/1.1142087.

[74] J. Bourret, N. Tessier-Doyen, B. Naït-Ali, F. Pennec, A. Alzina, C.S. Peyratout, et al., Effect of the pore volume fraction on the thermal conductivity and mechanical properties of kaolin-based foams, J. Eur. Ceram. Soc. 33 (2013) 1487–1495. doi:10.1016/j.jeurceramsoc.2012.10.022.

[75] G. Wei, X. Zhang, F. Yu, Thermal conductivity of xonotlite insulation

material, Int. J. Thermophys. 28 (2007) 1718–1729. doi:10.1007/s10765-007-0214-y.

[76] H. Salmang, H. Scholze, Keramik, 7th ed., Springer Berlin Heidelberg, 2007.

[77] W.D. Kingery, Thermal Conductivity: XII, Temperature Dependence of Conductivity for Single-Phase Ceramics, J. Am. Ceram. Soc. 38 (1955) 251–255.

LIST OF PUBLICATIONS

Publications in peer-reviewed journals:

1. S. Haastrup, D. Yu, Y.Z. Yue. Impact of surface impurity on phase transitions in amorphous micro silica, J. Non-Cryst. Solids 450 (2016) 42-47
2. S. Haastrup, M.S. Bødker, S.R. Hansen, D. Yu, Y.Z. Yue, Impact of amorphous micro silica on the C-S-H phase formation in porous calcium silicates, J. Non. Cryst. Solids. 481 (2018) 556–561
3. S. Haastrup, D. Yu, Y.Z. Yue, Impact of minor iron content on crystal structure and properties of porous calcium silicates during synthesis, Mater. Chem. Phys. 205 (2018) 180–185

Publication in conference proceeding and oral presentation:

4. S. Haastrup, B. Jørgensen, D. Yu, Y.Z. Yue. Impact of Micro Silica Surface Hydroxyl Groups on Calcium Silicate Products, 60th International Colloquium on Refractories (2017) 222–224

Oral presentation at conferences (abstracts):

5. S. Haastrup, D. Yu, Y.Z. Yue. Chemical fluctuation and phase transition in amorphous micro silica, The 24th international congress on glass (2016) p 153
6. S. Haastrup, D. Yu, Y.Z. Yue. Influence of iron on crystallization behavior and thermal stability of the insulating materials - porous calcium silicates, 12th Pacific Rim Conference on Ceramic and Glass Technology (2017)

ISSN (online): 2446-1636
ISBN (online): 978-87-7210-165-1

AALBORG UNIVERSITY PRESS